UNIVERSITY OF SOUTH BOHEMIA IN ČESKÉ BUDĚJOVICE

INSTITUTE OF PHYSICAL BIOLOGY

Zuzana SAJDLOVÁ

ELECTROCHEMICAL DETECTOR WITH ELECTRODES ARRAY AND ROTATING DISK

Ph.D. thesis

Supervisor: doc. RNDr. Jiří Masojídek, CSc., University of South Bohemia in České Budějovice

Expert supervisor: RNDr. Jan Krejčí, Ph.D., BVT Technologies, a.s.

BRNO, 2010

Anotace

Předkládaná disertační práce se zabývá testováním a optimalizací hydrodynamických podmínek elektrochemického detektoru, který sestává z průtočné cely, do níž se vkládá elektrochemický senzor s polem elektrod. Průtočná cela obsahuje rotační člen ve tvaru disku, který umožňuje radiální tok analyzované látky podél elektrod senzoru. Tento princip tedy napodobuje rotační diskovou elektrodu, s tím rozdílem, že zde jsou elektrody nepohyblivé. Hydrodynamické jevy jsou v tomto případě podobné s RDE. Proto se teoretická část práce podrobně zabývá hydrodynamikou a přenosem hmoty pro již popsaný případ rotační diskové elektrody.

V průběhu řešení bylo zjištěno, že ve stávajícím uspořádání dochází za určitých podmínek i při laminárním proudění ke zpětnému toku analytu z výstupního kanálu k senzoru. To způsobuje nelineární odezvu elektrod a jejich malou reprodukovatelnost. Řešením je podstatné snížení vzdálenosti mezi rotačním členem a povrchem elektrod a také snížení rychlosti proudění analyzované kapaliny k senzoru.

Byl navržen a otestován nový typ senzoru s elektrodami ve tvaru soustředných kruhů, který čtyřnásobně zvýšil konverzi analytu oproti původně testovanému senzoru AC9 s elektrodami ve tvaru plných kruhů ležících na společné kružnici. Využitím tohoto senzoru, upravením průtočné cely a snížením rychlosti vstupního toku lze dle výpočtů dosáhnout až 100% konverze analytu na rovinné elektrodě.

Detektor byl připojen ke kapalinovému chromatografu a jeho funkce byla testována na dvou látkách – kyselině askorbové a dopaminu. Pro stávající detektor byly stanoveny parametry: dynamický rozsah, linearita, šum, limit detekce, časová konstanta a rozsah teplot, ve kterém lze detektor provozovat.

Annotation

The thesis deals with the testing and optimization of hydrodynamic conditions of the electrochemical detector, which consists of a flow cell containing the electrochemical sensor with an array of electrodes. The flow cell includes a rotating disc-shaped component, which allows radial flow of analytes along the sensor electrodes. This principle imitates the rotating disk electrode, with the difference that here the electrodes are immobile. Hydrodynamic phenomena in this case are similar to RDE. Therefore, the theoretical part of my work deals with hydrodynamics and mass transfer for the well-described case of rotating disk electrode.

It was found that in the current set-up under certain conditions, an analyte flowed back from the output cell channel to the sensor, even at the laminar flow. This causes a nonlinear response of the electrodes and their low reproducibility. The solution is to reduce the distance between the rotation component and the electrodes surface and reduce flow speed of analyzed liquid towards the sensor.

A novel type of sensor with annular electrodes was designed and tested. It showed four times higher conversion rate of the analyte compared with the originally used AC9 electrochemical sensor having electrodes in the form of full circles lying on a circumference of a common circle. Based on calculations, conversion of the analyte on the plane electrode can be increased up to 100% when using this annular sensor, adjusting flow cell and reducing of the input flow rate.

The detector was connected to the liquid chromatograph and its function was tested on two substances - ascorbic acid and dopamine. For the current detector these parameters were set: dynamic range, linearity, noise, detection limit, time constant and the temperature range at which the detector can be operated.

Declaration on authorship / Čestné prohlášení o autorství práce

Prohlašuji, že svoji disertační práci jsem vypracovala samostatně pouze s použitím pramenů a literatury uvedených v seznamu citované literatury.

Prohlašuji, že v souladu s § 47b zákona č. 111/1998 Sb. v platném znění souhlasím se zveřejněním své disertační práce, a to v nezkrácené podobě elektronickou cestou ve veřejně přístupné části databáze STAG provozované Jihočeskou univerzitou v Českých Budějovicích na jejích internetových stránkách, a to se zachováním mého autorského práva k odevzdanému textu této kvalifikační práce. Souhlasím dále s tím, aby toutéž elektronickou cestou byly v souladu s uvedeným ustanovením zákona č. 111/1998 Sb. zveřejněny posudky školitele a oponentů práce i záznam o průběhu a výsledku obhajoby kvalifikační práce. Rovněž souhlasím s porovnáním textu mé kvalifikační práce s databází kvalifikačních prací Theses.cz provozovanou Národním registrem vysokoškolských kvalifikačních prací a systémem na odhalování plagiátů.

3.11.2010

Zuzana Sajdlová

Acknowledgement

Contents

1 Introduction

High performance liquid chromatography (HPLC) is probably the most universal type of analytical procedure; its application areas include quality control, process control, forensic analysis, environmental monitoring and clinical testing. In addition HPLC also ranks as one of the most sensitive analytical procedures and is unique in that it easily copes with multi-component mixtures [1]. HPLC utilizes a column that holds stationary phase, a pump that moves the mobile phase(s) through the column, and a detector that shows the retention times of the molecules. There are different detectors usually coupled with HPLC. Some of the more common detectors include: Refractive Index (RI), Ultra-Violet (UV), Fluorescent, Radiochemical, Electrochemical (ECD), Near-Infra Red (Near-IR), Mass Spectroscopy (MS), Nuclear Magnetic Resonance (NMR), and Light Scattering (LS) [2].

The presented thesis aims to design, develop and test low price electrochemical detector for HPLC based on a screen-printed electrochemical sensor with an electrode array. The detector will consist of flow cell and the sensor. The hydrodynamics in the sensor/cell system will be described and optimized. Detector specifications such as dynamic range, linearity, noise level, minimum detectable concentration, time constant, and operating temperature range will be measured.

The motivation of this thesis is using new knowledge and technologies to decrease the price for developed detector in 1-2 orders in comparison with usually used electrochemical detectors (ECD). It will enable spread of electrochemical sensors and make the HPLC/ECD analysis more available to research institutions and companies saving resources.

This thesis was carried out in the company BVT Technologies, a.s., where I am a full-time employee. In contrast to ordinary university students, I could not devote all my time to the dissertation and my limited publication activities had to be also focused to other topics of higher priority for my company. The thesis was worked out from the industrial point of view. The practical work was not limited to proof of principle but also preparation of results for their usage in practice, i.e. as a device or method. It explains the participation of my colleagues.

2 Theoretical part

Both different electrochemical detectors construction and analytical use is provided in the theoretical section. General parameters important to describe performance of any HPLC detector are defined first. Hydrodynamics for the simplest flow in tube towards liquid flow caused by rotating disk is explained further, because the research lies at the frontiers of knowledge of flow cell design, arrays of electrodes and mass transport aimed at improving electrochemical array detector response.

2.1 HPLC detectors parameters definition

Linear range

The ideal detector gives a signal with an area proportional to the amount injected, irrespective of whether it is large or small. Obviously, this linearity is not infinite but should embrace as wide range as possible. The slope of line drawn in Fig. 1 is known as response and represents the extent to which the detector reacts to a specific change in concentration [3].
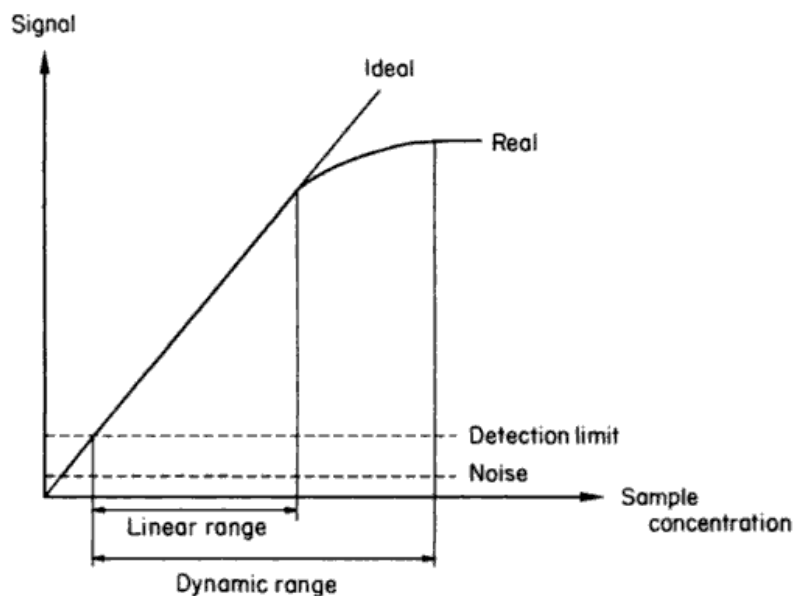
Fig. 1: Linear detector range [3].

Time constant

The time constant, τ, is a measure of the rate at which a detector can record a peak. As the detector works together with the data acquisition, the time constant of this combination is an important factor. The time constant can be defined as the minimum time required by a system to reach a 63% of its full-scale value (98% is also often specified). It should not be greater than 0.3 s for detecting very narrow HPLC peaks, i.e. those that are rapidly eluted at a volume of less than 100 µl, and should not exceed 0.1 s for high-speed HPLC. Too small a time constant increases noise level, but if it is too large the peaks become wide and tailed. Better-quality detectors offer a choice of time constant [3].

Cell volume

The volume of detector cell should have a negligible influence on a peak broadening and should, therefore, amount to less than 10% of the elution volume of the narrowest (first) peak. A cell of 8 µl is standard. Too small cell volume impairs the detection limit (as a certain amount of product is needed to produce any signal at all). The cell must have no dead corners which may prevent the peak being fully removed by subsequent eluent [3].

Detection limit

The smallest detectable signal cannot be less than double the height of the largest noise peak. For qualitative analysis the signal-to-noise ration should not be lower than 3-5; for quantitative analysis it must be higher than 10 [3].

Dynamic range

The dynamic range is a range of solute concentration over which the detector continues to respond to changes in solute concentration. It extends from the minimum detectable concentration to that concentration where the output no longer increases with a rise in solute concentration [1].

Noise level

Noise level is the signal recorded without sample in the cell. In HPLC, it is usually measured with water flowing through the cell [4].

Pressure and flow sensitivity

Pressure and flow sensitivity are to some extent interdependent. Both of them influence the long-term noise of the detector. They are usually measured as the change in detector output for unit change in the sensor pressure, resp. flow rate through the sensor [5].

Operating temperature range

Operating temperature range is the ambient temperature range over which the detector can be operated and maintain its specifications.

2.2 Electrochemical detectors for HPLC

Electrochemical detectors are used for their high selectivity when detecting reducible and oxidable compounds. These detectors are simple and low cost. The detector consists of three electrodes: working, reference and auxiliary electrode. Potential for the reaction is applied between working and reference electrode. The reaction of interest takes place on the surface of working electrode and is driven by the potential. Current produced by electrochemical reaction is balanced by current flowing in the opposite direction at the auxiliary electrode.

2.2.1 Principles of detection

Electrochemical reaction, at a solid surface electrode over which a liquid stream is flowing, is characterized by the following three separate stages:

1. Diffusion of the electroactive analyte to the electrode surface

2. Electron transfer as dictated by the electrochemical reaction

3. Diffusion of the reaction product(s) away from the electrode surface

During oxidation the electrochemical reaction gives rise to the release of electrons into the electrode (stage 2). This flow of electrons (current) is subsequently converted to a signal, which can be monitored by suitable circuitry (Fig. 2) [6].
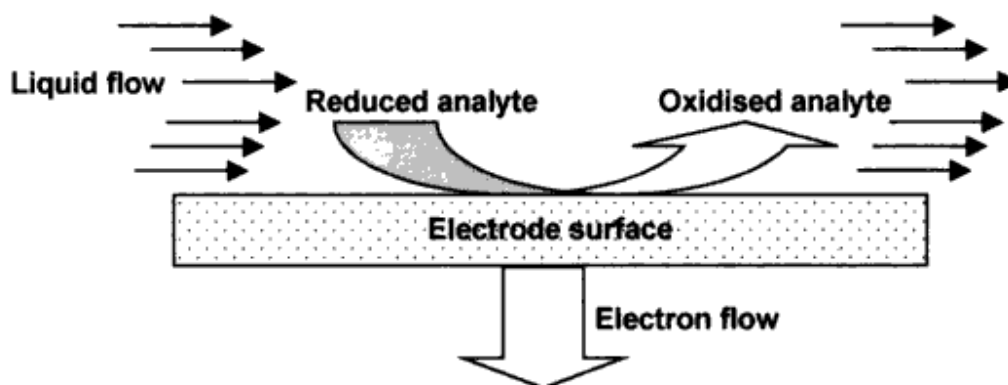
Fig. 2: Schematic diagram of the electrode processes occurring when, in this case, the reduced analyte flows over a static electrode held at an appropriate voltage [6].

Due to flow-induced mixing, the analyte is present at a constant concentration throughout the eluent bulk except for a narrow layer (thickness δ) immediately above the electrode surface. Only analyte molecules can diffuse to the surface in this relatively stationary layer. Consumption of the analyte, either by reduction or oxidation, created a concentration gradient. The thickness of the diffusion layer above the electrode is therefore critical to electrochemistry [6].

2.2.2 Flow cell design

Of the various EC detector cell designs (Fig. 3), the thin layer and wall jet configurations are commonly used in commercially available amperometric detectors, although it is possible to work coulometrically using a porous cell provided a large enough surface area is used. However, the trend appears to be towards smaller surface areas to make the detectors compatible with microbore HPLC systems and to reduce noise, which is proportional to surface area. Of the porous flow-through designs the most frequently encountered are the porous graphite type used in several ESA Coulochem detector cells. Tubular electrodes have not been commercially exploited and the single fibre electrode is chiefly confined to use with miniaturized systems and CE [6].
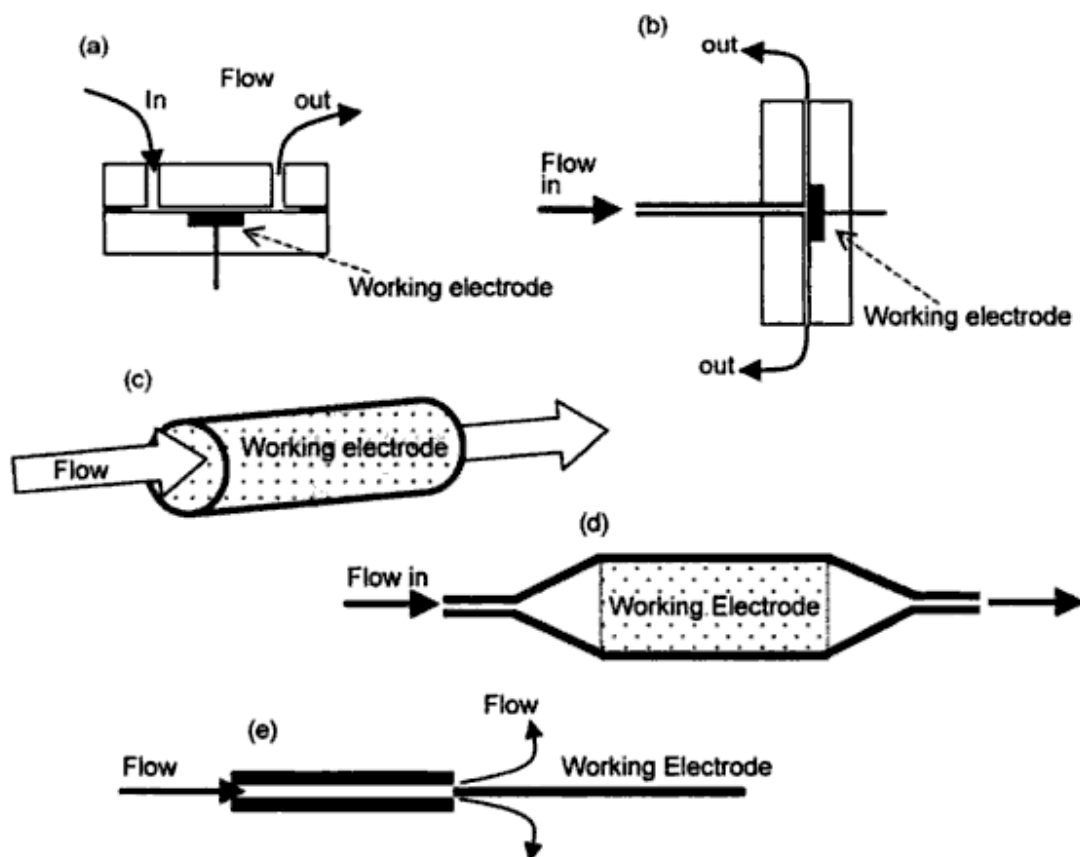
Fig. 3: Simplified designs of chromatographic ECD cells: (a) Thin/layer cell; (b) Wall jet cell; (c) Tubular cell; (d) Porous flow-through cell; (e) Single fibre electrode [6].

Wall-jet principle is used in the cell design in this work; therefore I put here more details about this type of cells. In wall-jet cells the eluate is delivered, via a small orifice, into the cell and directly impinges as a jet at the right angle onto the face (wall) of the electrode before radially flowing across the surface. The signal is dependent on the size of electrode and the diameter of the jet. Since the flow of electrolysed eluate is separated from the electrode, the design is intended to sweep the surface clean. High flow velocities are important. There are number of other critical factors to consider. It must be assumed that the jet does not break up before it hits the electrode. The jet is intact for a distance of up to 10 mm. Secondly, it is important not to restrict the radial flow from the zone where the jet impinges on the electrode. Finally, the electrode diameter should be at least ten-fold greater than the jet diameter [6].

2.2.3 Amperometric detector with a rotating disc electrode (RDE)

A rotating disc electrode is one of the best methods to obtain efficient mass transport in a highly reproducible manner. It consists of a cylindrical metal rod embedded in a larger cylindrical plastic holder. The electrode is cut and polished flush with its holder, so that only bottom end of the metal cylinder is exposed to the solution. The configuration of RDE is shown schematically in Fig. 4 [7].
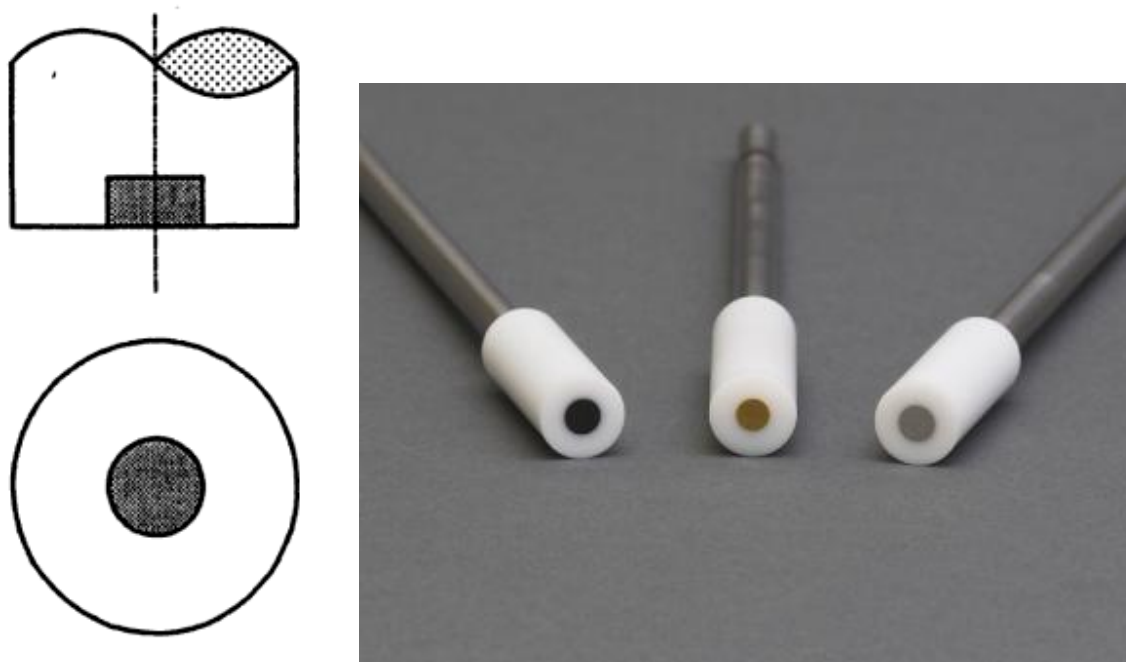
Fig. 4: The rotating disc electrode. The electrode and insulated material are marked by filled and clear areas, respectively [7]. Photograph – Pine Research Instrumentation.

The most important feature of the RDE is that it acts as „uniformly accessible surface", which in a simple language means that the rate of mass transport to the surface is uniform. Linear velocity of points on the surface increases with their distance from the centre of rotation. The other important property of RDE is that flow of the solution around is laminar up to rather high rotation rates. The transition from laminar to turbulent flow is characterised by dimensionless Reynolds number, *Re* [7].

Reynolds number is a product of a characteristic velocity v, by a characteristic length l, divided by kinematic viscosity v:

$$\text{Re} = v.l/v \tag{1}$$

In the case of rotating disc, the characteristic velocity is the linear velocity at the outer edge of the disc, given by v=ω.r, where ω is the angular velocity, expressed in radians per second. The characteristic length is radius r and the critical Reynolds number is about 1.10^5. The condition for laminar flow is then:

$$\text{Re} = (\omega.r)r/v = \omega.r^2/v < 1.10^5 \tag{2}$$

It should be noted that critical Reynolds numbers represent, as a rule, the upper limits for laminar flow at ideally smooth surfaces. If the surface is rough, turbulence may set in at a lower Reynolds number. For this reason most RDEs are set to operate at a maximum speed of 1.10^4 rpm (ω=1.10^3 rad/s, well within the range of laminar flow). The lower limit for the rotation rate is determined by the requirement that the limiting current density resulting from rotation be large compared to that which would exist in a stagnant solution due to natural convection. In practice this corresponds to a lower limit of about 400 rpm, which can be extended to 100 rpm under carefully controlled experimental conditions [7].

Since flow is laminar, it is possible to calculate rigorously the rate of mass transport. The corresponding equation for the limiting current density i_L, developed by Levich, is:

$$i_L = 0.62nFD^{2/3}v^{-1/6}\omega^{1/2}C^0 \tag{3}$$

The angular velocity in this equation is given in radians per second [7].

In amperometric detectors with a stationary electrode, the thickness of the diffusion layer mainly depends on the detector flow-cell geometry and on the flow rate through the detector. Flow rate variations are often caused by pumps that give rise to oscillating background. Additionally, a reduced sensitivity is anticipated at lower flow-rates, unless detector dimensions are adapted. The rotating disc electrode overcomes these limitations. At an RDE, the thickness of the diffusion

15

layer depends mainly on the rotation speed. Thus, in such a flow-cell it should be possible to maintain a minimal and constant diffusion layer, with elimination of the influence of the flow-rate [8].

The performance of the RDE may be affected by several variables, such as flow rate, rotation speed of the electrode and the height of the RDE in the flow cell above the eluent inlet (nozzle distance). The last parameter, the nozzle distance, may be a critical one in order to obtain maximum sensitivity and undistorted peak shape [8].

Under working conditions, the rotator movement of the electrode (up to 40 rps) does not increase the noise in the detector signal, provided the pulleys are properly grounded. If this is not the case, static electricity may accumulate on the pulleys, which causes irregular noise and makes detector sensitive to motions in its vicinity [8].

2.2.4 Electrochemical detectors analytical use

Electrochemical detectors can analyze so called electroactive species, i.e. substances that can be either oxidized or reduced. Such a substances can be found in following compound classes: amino acids, antioxidants, chlorinated anilines, chlorinated napthols, DNA adducts, drugs, flavonoids, general biochemicals, herbicides, phenols, hydroquinone conjugates, hydroxylated biphenyls, neurotoxins, PCB metabolites, polynuclear aromatics, ROS/RNS (reactive oxygen species/reactive nitrogen species), spin traps and vitamins [9].

Electrochemical detectors are ideal solution for a broad spectrum of analytical problems in following areas:

Pharmaceutical – from drug discovery to quality control electrochemical detectors enable measurement of small quantities of pharmaceuticals and their metabolites, even in complex samples. Applications include discovery of novel drugs in natural products, assessment of drug stability, and determination of physiological activity. Recent published works include:

- accurate determination of metoclopramide (blocks dopamine receptor and it also treats gut mobility disorders), hydrochlorothiazide (treatment of hypertension and oedema

associated with heart failure and with renal and hepatic disorders), imipramine (antidepressant) and diclofenac potassium (nonsteroidal anti-inflammatory drug) in serum or plasma samples [10],

- detection of tricyclic antidepressant drugs - imipramine, desipramine, clomipramine, amitryptyline and doxepin - by boron-doped diamond electrodes [11],

- simultaneous determination of diclofenac (opthalmopharmocological drug with anti-inflammatory, analgetic and antipyretic effects) and oxybuprocaine (anaesthetic drug in ophthalmology) in human aqueous humor [12],

- pharmacological studies of artesunate–amodiaquine drug combination for the treatment of falciparum malaria [13],

- quality control of positron emission tomography (PET) radiopharmaceuticals, namely analysis of [^{11}C]MP4A, useful for measuring acetylcholinesterase activity in the brain with no available UV absorbance [14],

- determination the concentration of diclofenac sodium in pharmaceutical formulations using a tubular bismuth film electrode [15],

- method for determination of biotin (vitamin H or B$_8$) in pharmaceutical preparations [16].

Food & beverage – Electrochemical systems are able to measure low levels of non-volatile flavonoids and phenolics. It can provide a competitive advantage by profiling the characteristic qualities of products, determining their integrity, and evaluating competitors' products. Publications from recent years cover:

- analysis of food colorants and potential carcinogens sudan I, sudan II, sudan III, and sudan IV by glassy carbon electrode and carbon nanotube-ionic liquid gel modified electrode [17],

- detection method for α-acids, β-acids and xanthohumol in hops. These substances are responsible for bitterness and taste of beer and xanthohumol exhibits also antioxidant action [18],

- simultaneous femtomole determination of cysteine, reduced and oxidized glutathione, and phytochelatin in maize; these substances eliminate oxidative stress in plants and play important role in heavy metal detoxification [19],

- detection of oil soluble antioxidant, carnosic acid, in meat and meat products [20],

- detection of catechin, epicatechin and epigallocatechin gallate (polyphenolic antioxidants plant secondary metabolites, flavoniods) [21].

Neuroscience – The measurement of neurotransmitters, simultaneous monoamines, and amino acids are just some of the examples of the neuroscience applications.

- sensitive electrochemical detection of DNA hybridization on an array based on DNA intercalators derived from naphtalenediimide appended with ferrocene reporter group [22],

- method of dopamine, L-dihydroxyphenylalanin, dihydroxyphenlyacetic acid and homovanillic acid detection that does not need derivatization or extraction step [23],

- fast determination of neurotransmitters aspartate and glutamate in microdialysis samples [24],

- flow-through detection of dopamine secreted from PC12 cells (cell line derived from a neuroendocrine tumor of the rat adrenal medulla) on microsensors [25],

- separation and quantisation of amphetamine and its metabolite, 4-hydroxynorephedrine applicable for the assay of substances in toxicology and drugs abuse [26].

Chemical & general purpose – Analysis in the environmental lab is enhanced by the ability to screen for a large number of compounds, such as pesticides and herbicides, where the allowable

limits are below those readily measurable by other then electrochemical analytical techniques. Recent examples to be mentioned:

- separation and detection of all six bromo- and chloro-acetic acids. Haloacetic acids are side products at water chlorination. [27],

- determination of thiamethoxam (neonicotinoid insecticide) residues in honeybees [28],

- electrochemical oxidation of aliphatic amines (air pollutants) derivatized with 2,5-dihydroxybenzaldehyde at porous graphite electrodes [29].

Oxidative metabolism – electrochemical systems are used in laboratories to determine everything from nutrition levels in foods to the study of free radicals in living organisms and their harmful effect on cells. It is an ideal analytical tool to study the often complicated multifaceted pathways involved in oxygen-protective mechanisms and damage that can result when those mechanisms fail.

- electrochemical detection approach used for quantisation of 8-hydroxy-2-deoxy-guanosine (8-OH-dG), DNA adduct that is a product of reactive oxygen species (ROS) reaction with cellular components such as proteins, lipids and nucleic acids [30],

- analysis of 3-nitrotyrosine in biological fluids and protein hydrolyzates to prove presence of peroxynitrite, which is responsible for tissue damage [31],

- useful protocol for the quantification of 3-nitrotyrosine in cells and tissues with aim to anticipate to fuel efforts in developing comprehensive inventories of nitrosative stress-induced protein-tyrosine modification sites in cells and tissues [32] ,

- protein-bound tyrosine that is used as biomarker for detection of reactive nitrogen species (RNS) significantly increased in near-term fetal rabbit brain following repetitive hypoxia-ischemia [33],

- accurate determination of ascorbic acid (AA), dehydroascorbic acid (DHAA) and uric acid (UA), in human plasma which is important for assessing their roles as biomarkers in disease diagnostics and evaluating oxidative stress [34].

I have added also below table to this chapter. It provides comparison of different detection modes used in HPLC for measurement of β-Carotene. Electrochemical detection is one of the best methods for the application.

Tab. 1: Comparison of Detection Limits and Reproducibility of Measurements (Relative Standard Deviations) for Various Detection Modes Used in HPLC of β-Carotene in Plasma and Serum [35].

Detection mode	Detection limit [mg.L-1]	Coefficient of variation [%]	Recovery [%]
UV/Vis, isocratic elution			
	12	9.3	101
	12	7.6	77
	6.5	6.4	-
	1.48	7.6	-
Gradient elution			
	7	3.4	100
	9.4	5.2	95
	1.5	5.6	99
Electrochemical			
	0.004 - 0.012	3-14	102
TLS			
	0.1	5	-
	0.58	4.1	101
Mass spectrometric			
APCI-MS	0.015	3	-
	0.003	5.4	102
ESI-MS	0.015	-	-
ESI-MS, NMR	0.0065	6.5	-

- data not given

2.2.5 The most commercially successful electrochemical detectors (ECD) for HPLC

Two Dionex-ESA products, i.e. Coulochem® Electrochemical Detector and CoulArray® Multi-Channel ECD system, are predominantly cited commercial electrochemical detectors for HPLC.

Both detectors use coulometric type of working electrode, which is a flow-through "frit" type porous graphite working electrode and is extremely efficient and capable of measuring 100%

electrochemically reactive species passing through it (Fig. 5B). The reason is simple: the porous electrode has large active surface. Even if the portion of the electrode is poisoned, still there is 100% analyte conversion. The signal does not depend on diffusion coefficient at 100% analyte conversion. The system can be calibrated easily then. Its response is given by Faraday law:

$$\int_0^T i(t)dt = nFQ\int_0^T C(t)dt.$$ (4)

The flow-through coulometric sensor is a highly efficient amperometric sensor with high selectivity [36].

Coulochem[®] III Electrochemical Detector contains DC potentiostat for 1 or 2 cells and potentiostat for guard cell and/or scan mode/pulse mode. Its price varies between 600 000 CZK and 1 200 000 CZK depending on accessories chosen.
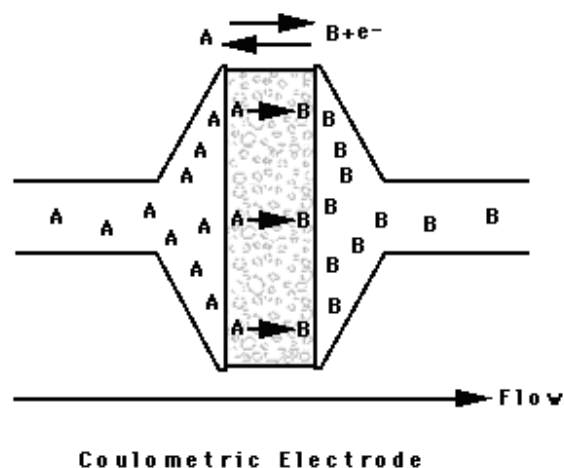
A   B

Fig. 5: A - Coulochem[®] III Electrochemical Detector picture, B - coulometric "frit" type electrode principle [37].

CoulArray[®] Multi-Channel ECD system bears 4, 8, 12, or 16 coulometric electrodes in series. It provides independent potential control for each electrode from -1 V to +2 V in one mV

increments. The CoulArray price varies from 900 000 to 2 500 000 CZK (including all accessories).

The producer declares: "The only practical multi-channel ECD system on the market, our CoulArray system allows you to measure multiple analytes simultaneously, including those that are chromatographically unresolved. The CoulArray delivers unmatched selectivity for the detection of trace components in complex matrices, even in the presence of co-eluting molecules."

Fig. 6: CoulArray® Multi-Channel ECD system [38].

2.3 Liquid flow in tube

Hydrodynamics general solution is still not available as Navier-Stokes equation (developed 1827-1845) understanding and proof belongs among Millennium Problems. Liquid flow in tube is one of the exceptional cases where the Navier-Stokes equations are solvable. The solution is Hagen-Poiseuille equation which was developed independently by Gotthilf Heinrich Ludwig Hagen and Jean Louis Marie Poiseuille. The latter experimentally derived and formulated the law in 1838 and it was published in 1840 and 1846. Hagen carried out his experiments in 1839 [39].

Velocity of liquid moving through the tube as a function of the distance from the centre of the tube is [39]:

$$v = -\frac{1}{4\eta}\frac{\Delta P}{\Delta x}\left(R^2 - r^2\right) \tag{5}$$

22

Poiseuille law for the total volume that flows through the tube is [39]:

$$Q = \frac{|\Delta P| \pi R^2}{8 \eta \Delta x} \qquad (6)$$

Electrode conversion/efficiency can be theoretically determined for tube case. Liquid flow through the tube of constant diameter can serve as the simplest model example allowing explicit results expression. Let's put a ring electrode of width d in the tube of diameter 2R (Fig. 7). The liquid velocity in the liquid layer of thickness δ from the electrode surface will be studied.
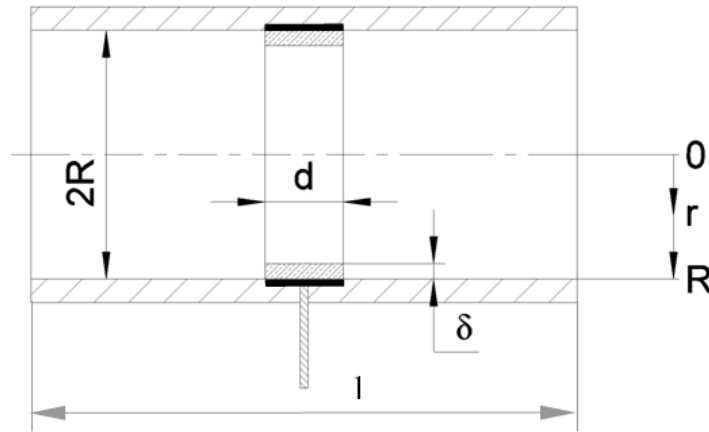
Fig. 7: Model of liquid flow very close to tube wall; electrode is represented by solid bold line

Let's assume that electrode reaction is much faster than diffusion processes. Then, following simple derivation is possible. The amount of liquid, which contains electroactive substance at concentration c, entering the ring of width d and thickness δ equals to substance flow towards electrode surface. As the area of very thin thickness δ is followed, the absolute value of flow J towards electrode surface can be expressed: $|J| = D.c/δ$. The concentration of electroactive liquid at the electrode surface equals to zero (due to electrode reaction assumption above). Concentration gradient at the electrode surface is approximated $c/δ$ on condition that electrode reaction proceeds at 100 % conversion. Then:

$$2\pi R\delta.v.C = d.2.\pi.R.|J| = d.2.\pi R.D.\frac{c}{\delta} \tag{7}$$

Velocity at the surface can be determined with the help of the Hagen-Poiseuille equation where the last term expresses the velocity in the half of the layer thickness.

$$v = \frac{\Delta p R^2}{4\eta d}\left(1 - \frac{(R - \delta/2)^2}{R^2}\right) \tag{8}$$

where Δp is pressure difference between input and output of the electrode area being of thickness d. This pressure difference can not be measured easily. As the pressure gradient is constant, we obtain: $\Delta p = (d/l).\Delta p_0$. Δp_0 is pressure difference between the tube beginning and end.

As δ is small, we can omit higher powers of δ.

$$v = v_0\frac{\delta}{R} - v_0\frac{\delta^2}{4R^2} \approx \frac{R\Delta p\delta}{4l\mu} \tag{9}$$

By substitution of velocity υ in the equation (7), we obtain:

$$2\pi R\delta.\frac{R\Delta p\delta}{4d\mu}.C = d.2\pi R.D.\frac{C}{\delta} \tag{10}$$

Equation (10) modification provides relation for layer thickness δ, which has crucial influence on sensor response.

$$\delta = \sqrt[3]{\frac{4Dd^2\mu}{R\Delta p}} \tag{11}$$

The current flowing through the electrode in such an arrangement:

$$I = d.2\pi.R.D.\frac{c}{\delta}.F.n \tag{12}$$

Integration of particular liquid ring layers inside the tube yields the total flow:

$$Q = \frac{\pi \Delta p_0}{4l\mu} R^4 \qquad\qquad (13)$$

The current corresponding to this liquid volume flow is:

$$I_0 = \frac{\pi \Delta p_0}{4l\mu} R^4.n.C.F \qquad\qquad (14)$$

Electrode conversion (efficiency) then depends approximately on geometry according to equation:

$$\frac{I}{I_0} \square\ 4.\left(\frac{d\mu D}{R^4 \dfrac{\Delta p_0}{l}} \right)^{2/3} \qquad\qquad (15)$$

The derivation shows how much electrode response depends on electrode geometry and liquid flow around them.

2.4 Liquid flow caused by rotating disk

Flow generated by disk rotation is an example, where approximate analytical solution can be found. The solution describes very well flow towards rotating disk in most usual experimental setups.

2.4.1 Infinite Plane Disk [40]

The equations for convective diffusion acquire their simplest form when the surface of rotating disk serves as the reaction site. The rotating disk is used in electrochemistry and is convenient for studying chemical kinetics under laboratory conditions. Von Karman and later Cochran have solved the problem in which liquid is entrained by a rotating disk whose axis is perpendicular to its plane surface. Cochran's exact solution of the hydrodynamic equations provides the following picture of the fluid motions. Far from rotating disk, the fluid moves toward the disk, and in a thin layer immediately adjacent to its surface, the liquid acquires a rotating motion. The angular velocity of the fluid increases as the surface of the disk is approached, until the angular velocity

of the rotating disk is finally attained. Furthermore, the fluid also acquires a radial velocity under the influence of the centrifugal force.

Further the principal considerations for determining the velocity distribution are presented. This problem is of special interest in hydrodynamics, because it is one of few examples where an approximate analytical solution of the hydrodynamic equations can be obtained. This solution gives the velocity distribution throughout the body of the viscous fluid.

The disk is assumed to be sufficiently large so that edge effects are negligible. In cylindrical coordinates the Navier-Stokes and continuity equations take the form [40]:

$$\frac{v_\varphi}{r}\frac{\partial v_r}{\partial \varphi} + v_r \frac{\partial v_r}{\partial r} - \frac{v_\varphi^2}{r} + v_y \frac{\partial v_r}{\partial y} = -\frac{1}{\rho}\frac{\partial p}{\partial r} + v(\Delta v_r - \frac{v_r}{r^2} - \frac{2}{r^2}\frac{\partial v_\varphi}{\partial \varphi}) \tag{16}$$

$$\frac{v_\varphi}{r}\frac{\partial v_y}{\partial \varphi} + v_r \frac{\partial v_y}{\partial r} + v_y \frac{\partial v_y}{\partial y} = -\frac{1}{\rho}\frac{\partial p}{\partial y} + v\Delta v_y \tag{17}$$

$$\frac{1}{r}\frac{\partial v_\varphi}{\partial \varphi} + \frac{\partial v_r}{\partial r} + \frac{v_r}{r} + \frac{\partial v_y}{\partial y} = 0 \tag{18}$$

where v_r, v_φ, and v_y are respectively, the radial, tangential, and axial velocity components respectively, and

$$\Delta = \frac{\partial^2}{\partial r^2} + \frac{1}{r}\frac{\partial}{\partial r} + \frac{1}{r^2}\frac{\partial^2}{\partial \varphi^2} + \frac{\partial^2}{\partial y^2} \tag{19}$$

At the surface of the disk the following boundary conditions must be satisfied:

$$v_r = 0, \ v_\varphi = \omega r \text{ and } v_y = 0 \text{ at } y = 0, \tag{20}$$

where ω is the angular velocity of the rotating disk. The condition on the tangential velocity component v_φ implies that the fluid near the disk rotates with it. Furthermore, the entrainment of fluid due to rotation of the disk leads to a significant radial velocity near its surface in a direction outward from the centre toward the edge of the disk. In order then that fluid may be continuously

supplied to the disk surface, an axial (vertical) flow must be maintained. Therefore, the boundary conditions at infinity are

$$v_r=0, \ v_\varphi=0 \ \text{and} \ v_y=-U_0 \ \text{as} \ y \rightarrow \infty. \tag{21}$$

The value of U_0 is determined from the solution of the problem itself. The minus sign indicates that the fluid velocity is toward the disk in the negative direction of the y axis. Due to axial symmetry, all derivatives with respect to the angle φ vanish. The pressure in the fluid may be considered constant along the radius r [40].

The hydrodynamics and diffusion derivation is very interesting from many aspects. The results are proven by 60 years of RDE usage, which is considered as the most precise electrochemical device. On the other hand some ideas of derivation are not correct. For example – infinite disk means that $v\varphi=\omega r$ and for $r \rightarrow \infty$ is true $v\varphi \rightarrow \infty$, which is impossible. Approximation connection, which leads to the final solution, is very instructive.

Then, equations may be rewritten as follows:

$$v_r \frac{\partial v_r}{\partial r} - \frac{v_\varphi^2}{r} + v_y \frac{\partial v_r}{\partial y} = \nu(\frac{\partial^2 v_r}{\partial y^2} + \frac{\partial^2 v_r}{\partial r^2} + \frac{1}{r}\frac{\partial v_r}{\partial r} - \frac{v_r}{r^2}) \tag{22}$$

$$v_r \frac{\partial v_\varphi}{\partial r} - \frac{v_r v_\varphi}{r} + v_y \frac{\partial v_\varphi}{\partial y} = \nu(\frac{\partial^2 v_\varphi}{\partial y^2} + \frac{\partial^2 v_\varphi}{\partial r^2} + \frac{1}{r}\frac{\partial v_\varphi}{\partial r} - \frac{v_\varphi}{r^2}) \tag{23}$$

$$v_r \frac{\partial v_y}{\partial r} + v_y \frac{\partial v_y}{\partial y} = -\frac{1}{\rho}\frac{\partial p}{\partial y} + \nu(\frac{\partial^2 v_y}{\partial y^2} + \frac{\partial^2 v_y}{\partial r^2} + \frac{1}{r}\frac{\partial v_y}{\partial r}) \tag{24}$$

Let´s seek a solution satisfying the continuity equation and the boundary conditions in the form

$$v_r = r\omega F(\xi), \ v_\varphi = r\omega G(\xi), \ v_y = \sqrt{\nu\omega}H(\xi), \ p = -\rho\nu\omega P(\xi) \tag{25}$$

(original hypothesis from T.v. Kármán [41]).

where the independent variable is the dimensionless quantity

27

$$\xi = \sqrt{\frac{\omega}{\nu}}\, y \tag{26}$$

and where F, G, H, and P are unknown functions which satisfy the equations

$$F^2 - G^2 + F'H = F'' \tag{27}$$

$$2FG + G'H = G'' \tag{28}$$

$$HH' = P' + H'' \tag{29}$$

$$2F + H' = 0 \tag{30}$$

and the boundary conditions

$$F=0,\ G=1,\ H=0 \text{ at } \xi=0, \tag{31}$$

$$F \to 0,\ G \to 0,\ H \to -\alpha \text{ as } \xi \to \infty, \tag{32}$$

all of which are obtained by substituting the definitions of v_r, v_φ and v_y into the Navier-Stokes and continuity equations, and into the boundary conditions. The constant $\alpha = U_0/\sqrt{\nu\omega}$ is to be determined.

The functions F, G and H may be made to satisfy the above equations and boundary conditions by formal series expansions. The nature of these expansions, for large values of ξ (asymptotic expansion), is suggested by the boundary condition for H. Thus, since the asymptotic value of H(ξ) is H$\to$-α as $\xi\to\infty$, and since the functions F and G become small as $\xi\to\infty$, it is possible to omit the quadratic terms in equation (27) and to rewrite it in the form:

$$-F'\alpha \approx F'' \text{ as } \xi\to\infty.$$

Integration of this equation yields the asymptotic expression for F

$$F \sim e^{-\alpha\xi} \text{ as } \xi\to\infty.$$

Similarly, as $\xi\to\infty$ equation (28) acquires the form

$$-G'\alpha \approx G'',$$

from which the asymptotic expression for G is

$$G \sim e^{-\alpha\xi} \text{ as } \xi \to \infty.$$

It follows that the asymptotic expansions of functions F, G and H must be exponentials of the form $e^{-\alpha\xi}$. The first terms of these expansions satisfying equations (16)-(19) and boundary conditions (31) and (32) are

$$F = Ae^{-\alpha\xi} - \frac{A^2+B^2}{2\alpha^2}e^{-2\alpha\xi} + \frac{A(A^2+B^2)}{4\alpha^4}e^{-3\alpha\xi} + ...,$$

$$G = Be^{-\alpha\xi} - \frac{B(A^2+B^2)}{12\alpha^4}e^{-3\alpha\xi} + ...,$$

$$H = -\alpha + \frac{2A}{\alpha}e^{-\alpha\xi} - \frac{A^2+B^2}{2\alpha^3}e^{-2\alpha\xi} + \frac{A(A^2+B^2)}{6\alpha^5}e^{-3\alpha\xi} + ...$$

In a similar manner, one can find expansions for small values of ξ satisfying the equations and boundary conditions:

$$F = \alpha\xi - \frac{\xi^2}{2} - \frac{1}{3}b\xi^3 + ...,$$

$$G = 1 + b\xi + \frac{1}{3}\alpha\xi^3 + ...,$$

$$H = -\alpha\xi^2 + \frac{1}{3}\xi^3 + ...$$

The constants A, B, a, b and α should be chosen so that the functions F, G, and H and derivatives F′ and G′ remain continuous when one matches these two series. Then the higher-order derivatives will also be continuous in accordance with the equations of motion. Numerical integration leads to the following values:

a = 0.51023, b = -0.616, α = 0.88447, A = 0.934, B = 1.208

The above described continuous connection of asymptotic solutions for $\xi \to \infty$ and $\xi \to 0$ is the key idea, which is a base of approximate analytical solution. The distribution of pressure P follows automatically. We shall later utilize the value of v_y, which to a first approximation is

$$v_y \approx -0.89\sqrt{v\omega} \text{ as } y \to \infty, \qquad (33)$$

$$v_y \approx -0.51(\sqrt{\omega^3/v}).y^2 \text{ for } y \Box \sqrt{v/\omega}. \qquad (34)$$

The functions F, G and H are shown graphically in Fig. 8. From the form of these plots, which decrease exponentially with increasing ξ, we obtain the following picture of the velocity distribution:
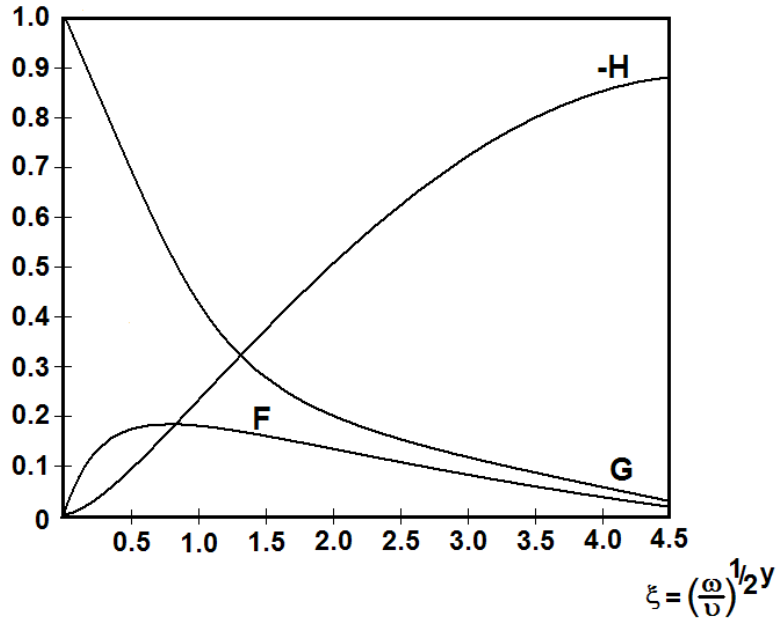

Fig. 8: Graphs of the functions F, G, and H [40].

at values of $\xi \approx 3.6$ (which corresponds to $y = \delta_0$), where

$$\delta_0 = 3.6\sqrt{\frac{v}{\omega}} \qquad (35)$$

v_y attains 80 % of its limiting value, and the velocity v_φ decreases to 0.05 times its value at the surface disk. Based on (35) and (25) the capture velocity of rotating disk can be evaluated:

$$U = 2\sqrt{\omega v}\int\limits_{0}^{3.6} F(\xi)d\xi \qquad (36)$$

Thus, in accordance with (35), we may regard δ_0 as defining the thickness of the hydrodynamic boundary layer on the disk surface. Within the boundary layer, the radial and tangential velocity components are not zero, while beyond that layer, only axial motion exists (Fig. 8). [Comment: The kinematic viscosity of water at 20^0C is 1.10^{-6} $m^2.s^{-1}$. Angular velocity at the rotation speed of 1200 rpm is 125 s^{-1}. The hydrodynamic boundary layer thickness is 320 μm, which is quite a large value. Small molecules have diffusion coefficient in magnitude of 10^{-10} $m^2.s^{-1}$. They diffuse through δ_0 in approx. 1000 s. Actual RDE response is approx. 10 ms.] The actual streamlines at the disk surface are shown in Fig. 9.
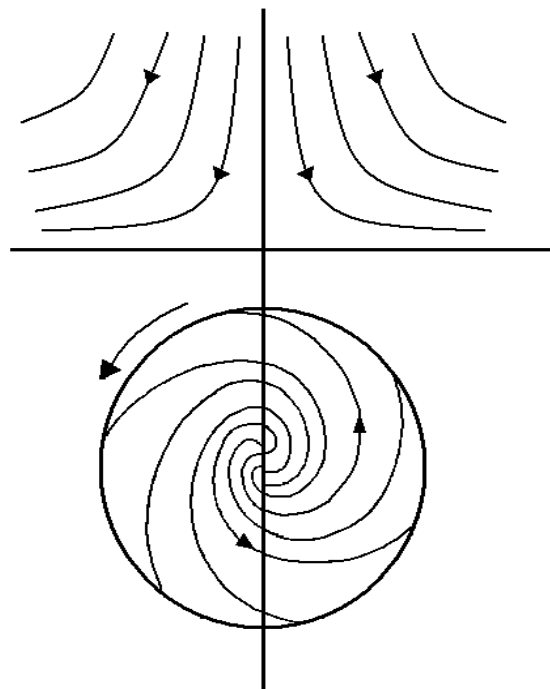

Fig. 9: Distribution of streamlines at the surface of rotating disk [40].

2.4.2 Disk of Finite Radius

Laminar flow. All the above considerations apply to a disk of infinite radius. However, for a circular disk of finite radius a that is much greater than the thickness of the boundary layer $\left(a \gg 3\sqrt{\upsilon/\omega} \right)$, these statements hold approximately, and so we can obtain some important practical estimates.

Using the capture rate of the fluid by the disk, $V_Z(\infty) = -0.886\sqrt{\upsilon\omega}$, one can find the rate of flow of the fluid captured by the disk of radius a and thrown away:

$$q = 0.886\pi a^2 \sqrt{\upsilon\omega^2}. \tag{37}$$

Since the disk is two-sided, the total rate of flow is in fact twice as large, $Q = 2q$. It is convenient to express the total rate of flow via the Reynolds number:

$$Q = 1.77\pi a^3 \omega \operatorname{Re}^{-1/2} \tag{38}$$

$$\operatorname{Re} = a^2 \omega / \upsilon. \tag{39}$$

In a similar way, one can estimate the frictional torque exerted by the fluid on the disk. It is given by the integral

$$m = -2\pi\mu \int_0^a \Re^2 \left(\frac{\partial V_\varphi}{\partial Z} \right)_{Z=0} d\Re. \tag{40}$$

For two-sided torque $M = 2m$, we have the estimate

$$M = 0.616\pi\rho a^4 \sqrt{\upsilon\omega^3}. \tag{41}$$

The dimensionless frictional torque coefficient is

$$c_M \equiv \frac{M}{\dfrac{1}{2}\rho a^5 \omega^2} = 3.87\operatorname{Re}^{-1/2}. \tag{42}$$

32

The theoretical estimate (42) is corroborated by experiments for the Reynolds number less than the critical value $\text{Re}_* \approx 3 \times 10^5$, at which the flow becomes unstable and a transition to the turbulent flow starts.

Turbulent flow. Approximate computations based on the integral boundary layer method lead to the following estimates for a disk of radius a in a turbulent flow $\left(\text{Re} > 3 \times 10^5 \right)$:

two-sided rate of flow is

$$Q = 0.438 a^3 \omega \, \text{Re}^{-1/5}; \tag{43}$$

the two-sided frictional torque coefficient is

$$c_M = 0.146 \, \text{Re}^{-1/5}. \tag{44}$$

The thickness of the turbulent dynamical boundary layer over the disk can be estimated by the formula $\delta = 0.5 a \, \text{Re}^{-1/5}$.

2.5 Diffusion to a rotating disk

2.5.1 Infinite Plane Disk [40]

We can now formulate the diffusion problem. The convective diffusion equation in cylindrical coordinates takes to form

$$v_r \frac{\partial c}{\partial r} + \frac{v_\varphi}{r} \frac{\partial c}{\partial \varphi} + v_y \frac{\partial c}{\partial y} = D \left(\frac{\partial^2 c}{\partial y^2} + \frac{\partial^2 c}{\partial r^2} + \frac{1}{r} \frac{\partial c}{\partial r} + \frac{1}{r^2} \frac{\partial^2 c}{\partial \varphi^2} \right) \tag{45}$$

The boundary conditions are

$$c = c_0 \quad \text{as} \quad y \to \infty, \tag{46}$$

where c_0 is the concentration in the bulk of the solution. For a maximum diffusion flux, the following condition prevails at the disk surface.

$$c = 0 \text{ at } y = 0. \tag{47}$$

Let's seek a solution of equation (45) satisfying boundary conditions (46) and (47) in the form:

$$c = c(y). \tag{48}$$

Let's assume that the concentration is a function only of distance from the disk surface and is not a function of either r or φ. Here we intentionally ignore effects at the edge of the disk where a solution in the form (48) cannot exist. Assuming that (48) is applicable, we rewrite equation (45).

$$v_y(y)\frac{dc}{dy} = D\frac{d^2c}{dy^2}. \tag{49}$$

By integrating (49) we obtain

$$\frac{dc}{dy} = a_1 \exp\left\{\frac{1}{D}\int_0^y v_y(z)dz\right\}, \tag{50}$$

and by second integration

$$c = a_1 \int_0^y \exp\left\{\frac{1}{D}\int_0^t v_y(z)dz\right\}dt + a_2. \tag{51}$$

The constants a_1 and a_2 are found from boundary conditions (46) and (47). The latter immediately yields

$a_2 = 0$, since, at $y = 0$, the integral (51) becomes zero. Also, because of boundary condition (46)

$$c_0 = a_1 \int_0^\infty \exp\left\{\frac{1}{D}\int_0^t v_y(z)dz\right\}dt. \tag{52}$$

In order to evaluate this integral, we can subdivide the interval of integration into two regions: from zero to δ_0 and from δ_0 to infinity, where δ_0, as defined by formula (35) is the boundary layer thickness. Beyond the boundary layer, v_y is given by formula (33). Within the boundary layer, v_y varies in a complex fashion. For high Prandtl numbers (i.e., for D ‹‹ v), the major variations

occurs in a region where distance from the solid surface is small compared to δ_0. For $y \lll \delta_0$, v_y may be approximated using equation (34). Below, we shall substitute for v_y its value form (34) and shall examine the justification for this step in the course of the calculations. Thus, we have:

$$J = \int_0^\infty \exp\left\{\frac{1}{D}\int_0^t v_y(z)dz\right\}dt = \int_0^{\delta_0} \exp\left\{\frac{1}{D}\int_0^t v_y(z)dz\right\}dt + \int_{\delta_0}^\infty \exp\left\{\frac{1}{D}\int_0^t v_y(z)dz\right\}dt = J_1 + J_2.$$

Using (34) and neglecting the higher order terms in the expansion of v_y we obtain for J_1

$$J_1 = \int_0^{\delta_0} \exp\left\{-\frac{\omega^{3/2}t^3}{5.88D\nu^{1/2}}\right\}dt.$$

Introducing a new variable

$$u = \frac{\omega^{1/2}t}{\sqrt[3]{5.88D^{1/3}\nu^{1/6}}}, \tag{53}$$

we find

$$J_1 \approx \frac{\sqrt[3]{6D^{1/3}\nu^{1/6}}}{\omega^{1/2}} \int_0^{\frac{\delta_0\omega^{1/2}}{\sqrt[3]{6D^{1/3}\nu^{1/6}}}} e^{-u^3} du = \frac{1.81D^{1/3}\nu^{1/6}}{\omega^{1/2}} \int_0^{2\left(\frac{\nu}{D}\right)^{1/3}} e^{-u^3} du.$$

For $\dfrac{\nu}{D} \ggg 1$, the upper limit of the integral is significantly greater than unity, and, since the integrand decreases rapidly for values of the argument greater than unity, we can replace the upper limit by infinity (for water at 20^0C is $\upsilon = 10^{-6}$, D for molecules of about 100 Dalton size is 10^{-10} m^{2}s^{-1}, $\upsilon/D = 10^4 \ggg 1$). Then

$$J_1 \approx \frac{1.81D^{1/3}\nu^{1/6}}{\omega^{1/2}} \int_0^\infty e^{-u^3} du.$$

35

Thus, because of the rapid convergence of the integral for $v \rangle\rangle D$, it is possible to use only the first term of the expansion of v_y. The magnitude of J_1 is determined chiefly by the small values of u. The integral for J_1 may now be expressed in terms of the Γ function,

$$\int_0^\infty e^{-u^3} du = \frac{1}{3} \int_0^\infty e^{-t} t^{-2/3} dt = \frac{1}{3} \Gamma\left(\frac{1}{3}\right) = \Gamma\left(1+\frac{1}{3}\right) = \Gamma\left(\frac{4}{3}\right) \approx 0.89.$$

Therefore, finally

$$J_1 = 1.6166 \frac{D^{1/3} v^{1/6}}{\omega^{1/2}}$$

The integral J_2 is computed in a similar manner:

$$J_2 = \int_{\delta_0}^\infty \exp\left\{\frac{1}{D}\int_{\delta_0}^t v_y(z)dz\right\}dt = \int_{\delta_0}^\infty \exp\left\{-\frac{0.89\sqrt{v\omega}}{D}t\right\}dt = \frac{D}{0.89\sqrt{v\omega}}\exp\left\{-\frac{0.89\sqrt{v\omega}}{D}\delta_0\right\} \cong \frac{D}{0.89\sqrt{v\omega}}e^{-3\left(\frac{v}{D}\right)}.$$

For $v \rangle\rangle D$, the value of the integral J_2 is very small compared to J_1 and can be omitted. Thus $J \approx J_1$ and from (52) we find that $a_1 = \frac{c_0}{J_1}$.

Finally for a concentration distribution that satisfied both the convective diffusion and the boundary conditions, we obtain

$$c = \frac{c_0}{J_1}\int_0^y \exp\left\{\frac{1}{D}\int_0^t v_y(z)dz\right\}dt = \frac{c_0}{1.61\left(\frac{D}{v}\right)^{1/3}\sqrt{\frac{v}{\omega}}}\int_0^y \exp\left\{\frac{1}{D}\int_0^t v_y(z)dz\right\}dt. \tag{54}$$

In order to determine c as function of distance y from the surface of the disk (where y=0) for small values of y (in comparison with δ_0) , we substitute v_y in (54) by its definition from (34). Then the equation for the concentration distribution (for y ‹ δ_0) can be written in a symmetrical form

$$c = c_0 \frac{\displaystyle\int_0^Y e^{-u^3}\,du}{\displaystyle\int_0^\infty e^{-u^3}\,du}, \tag{55}$$

where u is defined, as before, by formula (53) and Y denotes the ration

$$Y = y : \frac{\sqrt[3]{6} D^{1/3} v^{1/6}}{\omega^{1/2}} \approx \frac{2y}{\delta_0}\left(\frac{v}{D}\right)^{1/3}.$$

Equation (55) shows that for small values of y, the concentration increases very rapidly with the distance y (more rapidly than exponentially).

In a view of rapid convergence of the integral for Y>1, i.e. for $y \rangle \frac{1}{2}\left(\frac{D}{v}\right)^{1/3}\delta_0$, Y can be replaced by infinity, and the value of concentration in equation (55) reduces to c_0 (i.e., to the concentration in the bulk of the solution).

Differentiating (55) we obtain the mass flux to the disk surface

$$j = D\left(\frac{\partial c}{\partial y}\right)_{y=0} = \frac{Dc_0}{0.89} \frac{\omega^{1/2}}{\sqrt[3]{6}D^{1/3}v^{1/6}} = \frac{Dc_0}{1.61\left(\frac{D}{v}\right)^{1/3}\sqrt{\frac{v}{\omega}}} = 0.62 D^{2/3} v^{-1/6} \omega^{1/2} c_0. \tag{56}$$

Expressions (55) and (56) are in full agreement with the general considerations. The thickness of the diffusion boundary layer, represented by δ, is given by

$$\delta = \frac{Dc_0}{j} = 1.61\left(\frac{D}{v}\right)^{1/3}\sqrt{\frac{v}{\omega}} \approx 0.5\left(\frac{D}{v}\right)^{1/3}\delta_0. \tag{57}$$

The major change in concentration occurs in a region ~δ in thickness. For the usual values of the diffusion coefficient $D \sim 10^{-5}$ cm^2.s^{-1} in water, and for $\upsilon \sim 10^{-2}$ cm^2.s^{-1}, the thickness δ of the diffusion boundary layer constitutes only 5% of the thickness δ_0 of the hydrodynamic boundary

layer. This fully justifies the use of (34) for v_y instead of full expansion which holds for all values of y.

A significant characteristic of the diffusion boundary layer on a disk is the fact that its thickness is not a function of the distance from the axis of rotation, but is constant over the entire disk surface. The only exception is the zone at the edge, to which the foregoing analysis does not apply. The extent of this zone in which the edge of the disk does exert an effect apparently extends over a distance of δ_0.

Equation (56) shows that the diffusion flux to the surface of the disk is proportional to the 2/3 power of the diffusion coefficient D, to the (-1/6) power of the kinematic viscosity, and to the ½ power of the angular velocity. The flux is a function of kinematic viscosity according to the law $j\sim\upsilon^{-5/6}$. The total flow of matter to the disk surface is

$$I = \frac{\pi D c_0 R^2}{1.61\left(\dfrac{D}{\nu}\right)^{\!1/3}\sqrt{\dfrac{\nu}{\omega}}} \approx 1.9 D^{2/3}\nu^{-1/6}\sqrt{\omega}R^2 c_0. \tag{58}$$

Now we examine the effect of temperature on the diffusion flux to the disk. The diffusion coefficient D and the kinematic viscosity ν for the usual liquids are exponential functions of temperature:

$$D = D_0 e^{-\frac{U_D}{kT}}, \tag{59}$$

$$\nu = \nu_0 e^{+\frac{U_\nu}{kT}}, \tag{60}$$

where U_D and U_υ are, respectively, the activation energies for diffusion and viscosity, and D_0 and υ_0 relate to a reference temperature such as room temperature. The numerical values of U_D in most cases are approximately 13 kJ.mol^{-1}, and U_υ, somewhat greater, is about 15 kJ.mol^{-1}.

Substituting the expressions for D and υ into (56), we obtain

$$j \approx e^{-\frac{4U_D+U_\nu}{6kT}}. \tag{61}$$

Let us stress that all equations in this section apply only to laminar flow past the disk. Laminar flow is ordinarily sustained up to Re $\sim 10^4$, but with very well polished and centred disks up to Re $\sim 10^5$. On the other hand, at lower rotation speeds (Re ≈ 10), the thickness δ_0 of the hydrodynamic layer becomes comparable to the radius of the disk.

Use of a series for the function H(ξ) makes it possible to compute the value of v_y with any desired number of terms on the expansion in ξ.

Substituting the expression for v_y into (52) and including the higher-order terms of the expansion in the function H(ξ), we obtain, with an accuracy to terms of the third order,

$$J_1 \approx 1.61 \left(\frac{D}{\nu}\right)^{\frac{1}{3}} \sqrt{\frac{\nu}{\omega}} \left[1 - 0.35\left(\frac{D}{\nu}\right)^{0.36}\right]. \tag{62}$$

The value of integral J_1 is thus found to be somewhat greater than given by the zero approximation. Correspondingly, the total mass flow I is found to be somewhat smaller. The correction to the flux, given approximately by (58), is from three to five percent. Experimental values are given more closely by (58) than by (62). This means that there are additional corrections of the same magnitude but opposite in sign. One of them is for edge effect. The maximum value of this correction apparently occurs for a static medium. The flowing fluid always carries matter away from the edge of the disk. If the disk has an outer rim, then the flux to the disk is given by the equation

$$I' = 4RDc_0 \text{ and } \frac{I'}{I} = \frac{4}{\pi}\frac{\delta}{R} = 1.99\left(\frac{D}{\nu}\right)^{1/3}\sqrt{\frac{\nu}{\omega R^2}}.$$

Other correction to the flux toward the disk, which increases its value beyond that given by (58) are associated with natural convection and with the appearance of turbulence. The first correction becomes significant at small Reynolds numbers, and the latter at high Reynolds numbers. If a deposit forms on the disk surface, it grows for the most part at the edge, and the error of formula (58) increases [40].

2.5.2 Disk of Finite Radius [42]

The mean Sherwood numbers for a disk of finite radius a at high Schmidt numbers can be estimated using formula

$$Sh = 0.62 \, \mathrm{Re}^{1/2} \, Sc^{1/3}, \tag{63}$$

where the Reynolds number is determined from the relation $\mathrm{Re} = a^2 \omega / \upsilon$. The corrections that take account of the boundary effects result in quite small variations in the nuzmeric factor in (63) (within 5%).

Relation (63) is valid in the region of laminar flow past the disk; the laminar regime occurs until $\mathrm{Re} \approx 10^4$ to 10^5, depending on the roughness of the surface. For low Reynolds numbers ($\mathrm{Re} \leq 10$), this relation is invalid, because the thickness of the hydrodynamic boundary layer becomes comparable with the disk radius and the boundary effects on the hydrodynamic flow and mass transfer become stronger.

In the turbulent regime of flow, the mean Sherwood number for a disk of finite radius a can be approximated by the formula

$$Sh = 5.6 \, \mathrm{Re}^{1.1} \, Sc^{1/3}, \tag{64}$$

which is suitable for practical calculations for $6 \times 10^5 < \mathrm{Re} < 2 \times 10^6$ and $120 < Sc < 1200$ [42].

2.6 Improving the mass transfer along the sensor with array of electrodes

BVT Technologies, a.s. participated in the EU project Intellisens (QLK3-2000-01481), the aim of which was to create a methodology for fast monitoring of pollution levels in wastewater and pollution incidents based on a biosensor array-pattern recognition system. Problems to eliminate the crosstalk between electrodes of the array and ensure reproducible mass transport to each electrode appeared during the project solution. To solve it, Tautgirdas Ruzgas and Jan Krejčí invented the use of disk rotator with the analyte delivery through rotator axis (CZ patent 301131

and WO2004040292). The article of Eva Dock et and collaborators proved the principle of rotator with the channel for liquid [43]. They studied amperometric cell enabling steady-state and flow injection measurements on screen-printed arrays consisting of eight electrodes distributed radially. Dependence of electrode current as a function of distance between rotator and array was examined and it was found that the more narrow the better. Optimal distance was set to 1 mm. Optimal angular frequency of the rotator owing to the best current signal/noise ratio was found to be 15 Hz. The flow cell shown in this paper was in fact a steady-state cell with flow channel through rotator. The critical factor, limiting the reproducibility of the measurements was the manual positioning of the array into the cell.
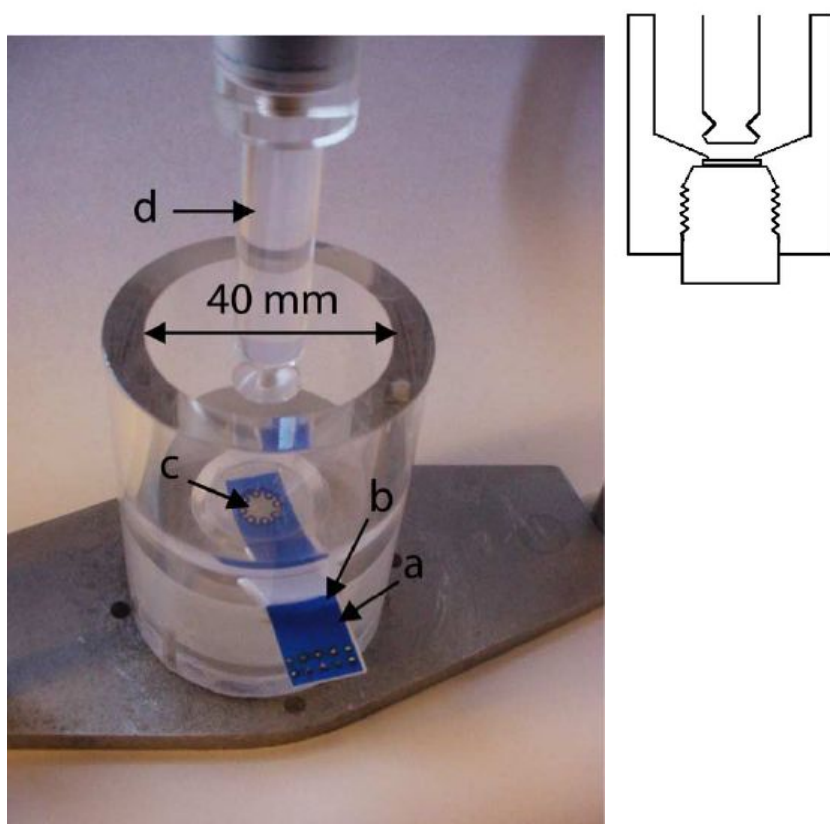

Fig. 10: Photograph of the amperometric steady-state cell made of Plexiglas. The array (a) is inserted into a rectangular hole (b) and the electrode surfaces are centred manually in the hole (c) at the bottom of the cell. The array is tensed in the cell via a screw, where some silicon is applied under the bottom hole (c) to keep the contact between the array surface and the cell watertight. An adjustable rotator (d) mixes the solution tightly over the array surface. (B) Cross-section view of the steady-state cell [43].

A new cell construction with user independent positioning of the screen printed arrays is described in experimental section

2.7 Summary

State of the art analysis was made with the aim to follow original ideas of Levich, Cochran and Karman on liquid flow and diffusion to rotating disk. Limiting hypotheses were found. They are:

1. the approximation by infinite rotating disk,

2. the constant velocity in y direction at infinity, which allows deriving equation (36).

The key ideas behind Levich equation derivation:

1. continuous and smooth connection of asymptotic solution for $\xi \rightarrow \infty$ and $\xi \rightarrow 0$,

2. equations (25) that are a priori set up on a physical insight into problem without any additional physical reasons. Validity proof of these equations by Lie groups was not successful.

Previous text proved the RDE potential in analytical applications. The possibility to analytically describe the mass transfer between bulk solution and the electrode surface enable RDE characterization. This is unappreciable RDE advantage especially because the mass transport influences the electrode response, which is underestimated problem of electrochemistry.

Experimental and results and discussion parts will apply the above ideas and try to use the general principles described above to exploit RDE principle to electrode array made by screen printing.

3 Objectives

The presented thesis aims to design, develop and test low-price electrochemical detector for HPLC based on a screen-printed electrochemical sensor with an electrode array. The detector will consist of flow cell and the sensor.

The hydrodynamics in the sensor/cell system will be described and both the rate of liquid flow and the speed of rotating magnetic element will be optimized to reach the same response for all electrodes in the array.

Detector specifications such as dynamic range, linearity, noise level, minimum detectable concentration, time constant and operating temperature range are to be measured.

Rotating disk electrode principle and unique properties will be applied on array of electrodes.

Analyte radial flow will be used to minimize a crosstalk between particular electrodes of the array.

Mass transfer towards electrodes surface will be improved so that the electrodes will work with higher conversion rate than usual amperometric electrodes.

New sensors with annular electrodes will be created characterized by low price and comparable characteristics to coulometric electrodes used in CoulArray®.

4 Experimental part

The aim of this part was to describe and test a novel electrochemical detector for HPLC analysis. The detector consists of electrochemical sensor with an array of electrodes AC9.W*.R* and a FC9 cell (both produced by of BVT Technologies, a.s., Brno, Czech Republic) designed to provide uniform mass transfer across all electrodes. The response of each electrode of AC9 array sensor was tested to determine the FC9 flow cell function. Static conditions were followed to study diffusion processes at the vicinity of electrode. Dynamic conditions (i.e. liquid flow and rotation of mixing element above electrodes) were tested at various regimes to follow kinetics and hydrodynamics of the FC9 cell. Liquid flow and mixing element rotation speeds were optimized for the flow cell to give similar response at all electrodes of the 8-electrode AC9 sensor. At the end the cell with AC9 sensor was connected to liquid chromatograph and a case study was performed on model substances - ascorbic acid and dopamine.

4.1 New construction of the cell

The electrochemical cell FC9 (further referred as FC9) was designed as a part of detector including the AC9 sensor, which bears eight electrodes array surrounded by common reference electrode (Fig. 11). Each electrode can be polarized to different potential. Mutual influence of electrodes is suppressed by radial flow of analyzed liquid (Fig. 11). Special multipotentiostat is needed to enable polarization and simultaneous measurement of eight electrodes. As such a multipotentiostat was not available; all the experiments were done on electrodes in sequence, not at one time.
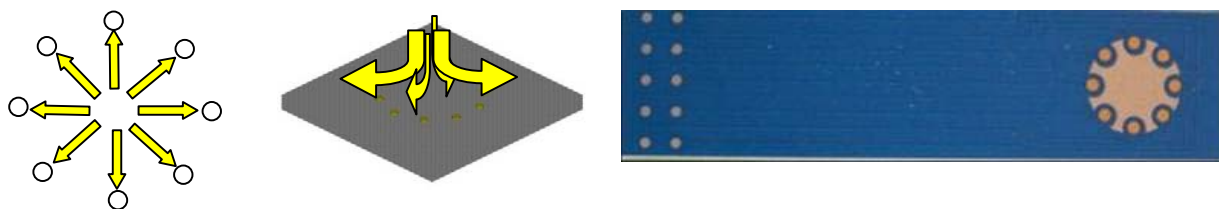

Fig. 11: Radial flow of liquid towards electrodes of array sensor; AC9.W1.RS electrochemical sensor with array of 8 working electrodes and one common reference electrode (BVT Technologies, a.s., Brno, Czech Republic)

The principle of rotating disc electrode was employed. In the FC9 flow cell the electrodes are stationary; the sensor is static with a hole in the middle of the electrodes circle structure. The rotation component distributes analyzed liquid from the middle of the electrodes towards edges, i.e. causing radial flow. Revolution transfer is done by magnetic field. Magnetic field is closing up in the rotation element what minimizes influence on electrodes (Fig. 12).
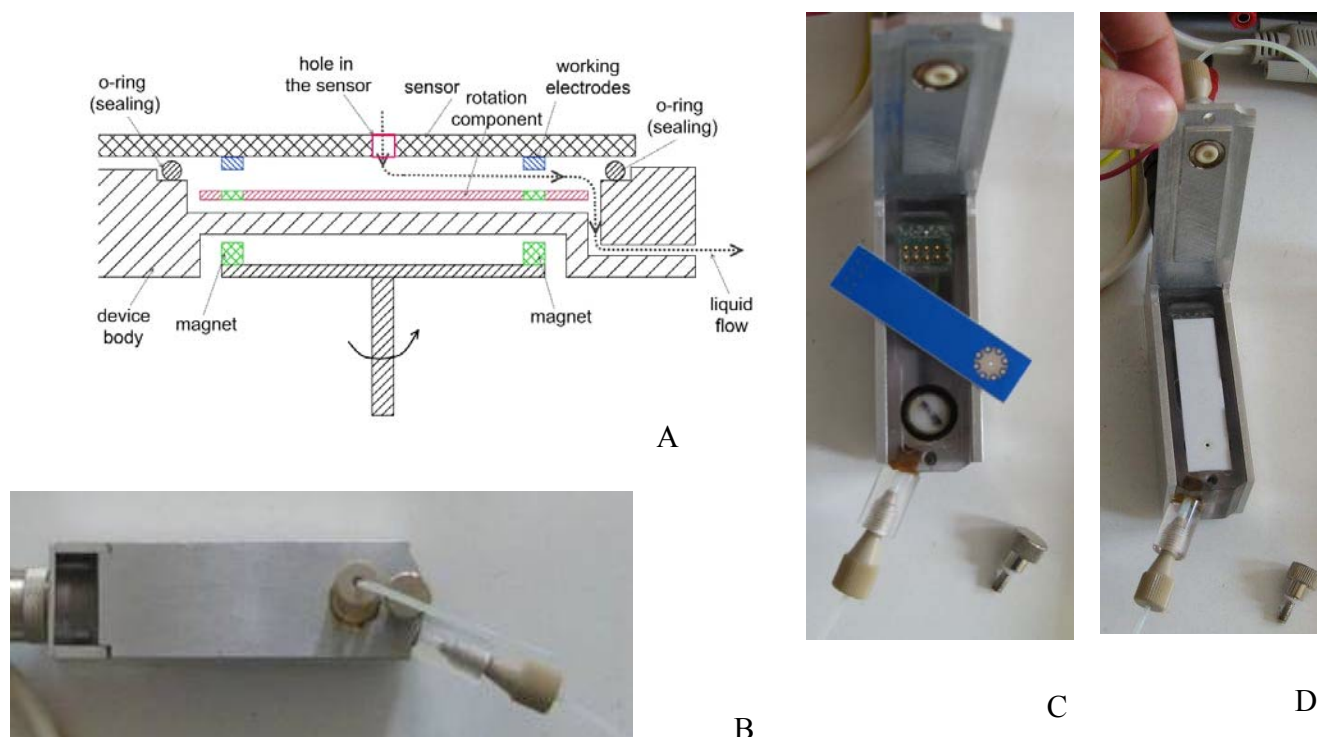

Fig. 12: Flow cell FC9 design: A – schematic diagram; B - photograph of closed cell; C - photograph of opened cell and D – photograph of the AC9 sensor inserted in the FC9 cell.

4.2 Dynamic conditions optimization

The aim of these experiments was to optimize both the rate of liquid flow and the speed of rotating magnetic element to reach the same response for all electrodes in the array.

The rotating component had a shape of a disk with a diameter of 9.8 mm and a thickness of 3 mm. I looked for an optimal combination of the rotation speed and the rate analyzed liquid flow to get the similar value of signal from all eight electrodes of the sensor. Nine AC9.W2.RS array

sensors (with 8 platinum working electrodes and 1 common reference silver electrode) were tested using an apparatus showed in Fig. 13.
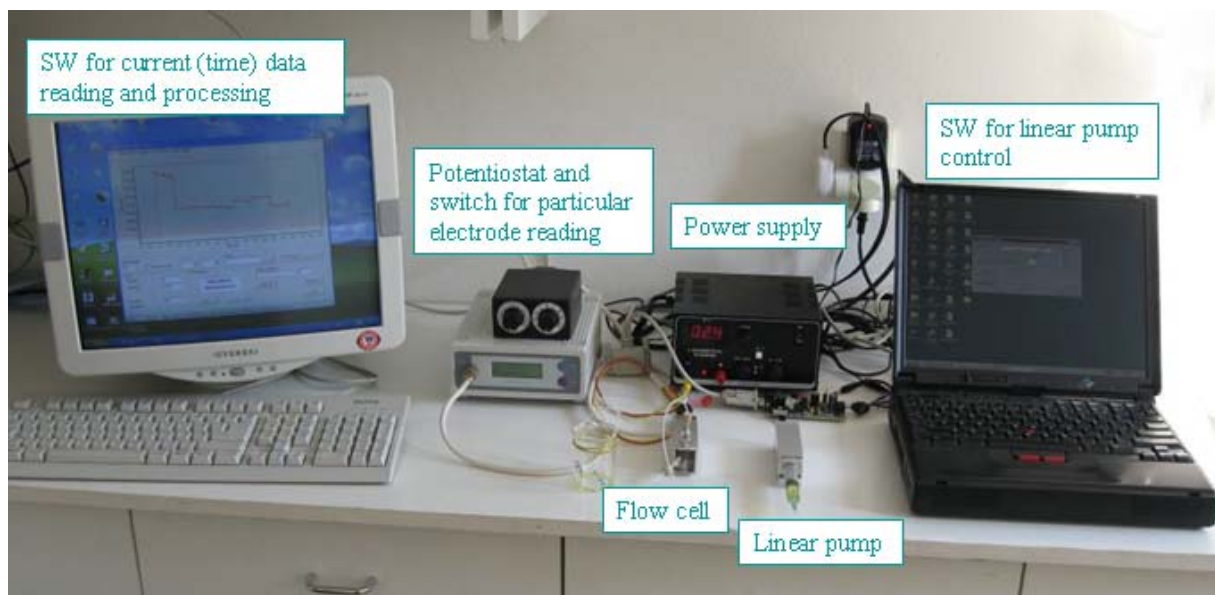

Fig. 13: Measurement set-up consists of the FC9 flow cell with the AC9 electrochemical sensor, linear pump LP controlled by Rizot® software, a power supply for rotating component, a switch for particular electrode reading, a BA1 potentiostat and Bioanalyzer software that enables data processing. Except a power supply, all named device are produced by BVT Technologies, a.s., Brno.

The rotation speed was regulated by a power supply. The voltage from the power supply to the motor of the rotation element was varied from 1.1 to 2 V; the voltage step was 0.1 V. The corresponding rpm/rps values are provided in Tab. 2.

Tab. 2: Applied voltage versus revolutions per minute/revolutions per second

Voltage [V]	rpm	rps
1.1	2017	34
1.2	2400	40
1.3	2817	47
1.4	3267	54
1.5	3750	63
1.6	4267	71
1.7	4817	80
1.8	5400	90
1.9	6017	100
2	6667	111

The flow rate of analyzed liquid from the linear pump was gradually increased in sequence: 50, 100, 150 and 200 µl/min. Electrochemical method used was amperometry.

4.3 Modelling the flow around sensor electrodes

There are three very important parameters of the novel detector consisting of array sensor AC9 and FC9 flow cell that define the flow velocity around the electrodes. These are distance between rotation component and sensor electrodes, flow rate in the input tubing and rotation component rotational speed. These three parameters were combined using Multiphysics Modeling and Simulation Software COMSOL to reach hydrodynamic characteristics of the system. Models were done for the rotation component – sensor electrodes distance of 0.1 and 0.2 mm, flow rate of 100 µl/s and 200 µl/s and rotation component rotational speed 0 and 100 rps.

4.4 Array sensor with increased conversion

Electrochemical sensors AC9.W*.R* presented in this work have the highest electrode reaction conversion of 3.7%. There was developed a new electrode design of the planar array sensor to compete coulometry. (Coulometry is characterized by 100% conversion.) The electrodes are not dots (like AC9 sensors) but concentric circles. Thus all liquid flowing from the middle of the sensor electrode part has to pass along electrode surface. For the first time this new design is presented in this thesis. It consists of 3 gold working electrodes and of 3 silver reference electrodes. The working and reference electrodes are designed so that they have the same geometric surface. The silver reference electrodes shield working electrodes. Thus the crosstalk between working electrodes is removed.

Fig. 14: Array sensor with annular electrodes of the same geometric area

The sensor was inserted in the FC9 flow cell. Flow rate of 0.005 M ferro-ferricyanide from the linear pump was 200 μl/min and voltage applied on rotation element was 1.9 V, i.e. 6017 rpm.

4.5 Case study

Performance of the electrochemical detector consisting of FC9 flow cell with AC9 array sensor and BA1 potentiostat (BVT Technologies, a.s., Brno) was tested through connection to liquid chromatograph SHIMADZU LC-10AS (Institute of Analytical Chemistry, Czech Academy of Science in Brno, Czech Republic). Ascorbic acid (AA) and dopamine (DA) were chosen as substances to be analyzed as they are electroactive and have often been determined by electrochemical detectors (for references see Chapter 2.2.4).

Material and Methods

LC Column: Eclipse XDB-C18 5 μm, 4.6 x 150 mm, Agilent product No.: 993967-902

Mobile phase: 0.1% (v/v) HCOOH (aq); pH = 2.2.

Flow rate: 1 ml/min.

Temperature: ambient.

Injection volume: 20 μl.

Detector: Bioanalyzer BA1.S (potentiostat), FC9 flow cell and AC9.W2.RS screen printed array of eight planar platinum electrodes.

Cell potential: E = +300 mV.

Working AA and DA solutions were prepared daily in deionised water from salt purchased from Sigma-Aldrich: H 8502 Dopamine hydrochloride, A 7506 L-Ascorbic acid.

5 Results and Discussion

5.1 Dynamic conditions optimization

Optimal combination of the flow rate and rotation speed was 100 μl.min^{-1} and 6667 rpm, respectively. It was found to have the smallest deviation between currents measured on all electrodes of all sensors. The deviation was 38.5%, which is very high. The reason can be non uniform spread of liquid over the particular electrodes of an array or different active surface of particular electrodes. The second mentioned reason is less probable according to experiments performed in BVT Technologies, a.s. The main weakness of electrochemical sensors that causes poor measurement reproducibility is undefined mass transfer. It is underestimated problem for most users of electrochemical sensors. The real active electrode surface is not completely used due to insufficient mass transfer towards electrode.
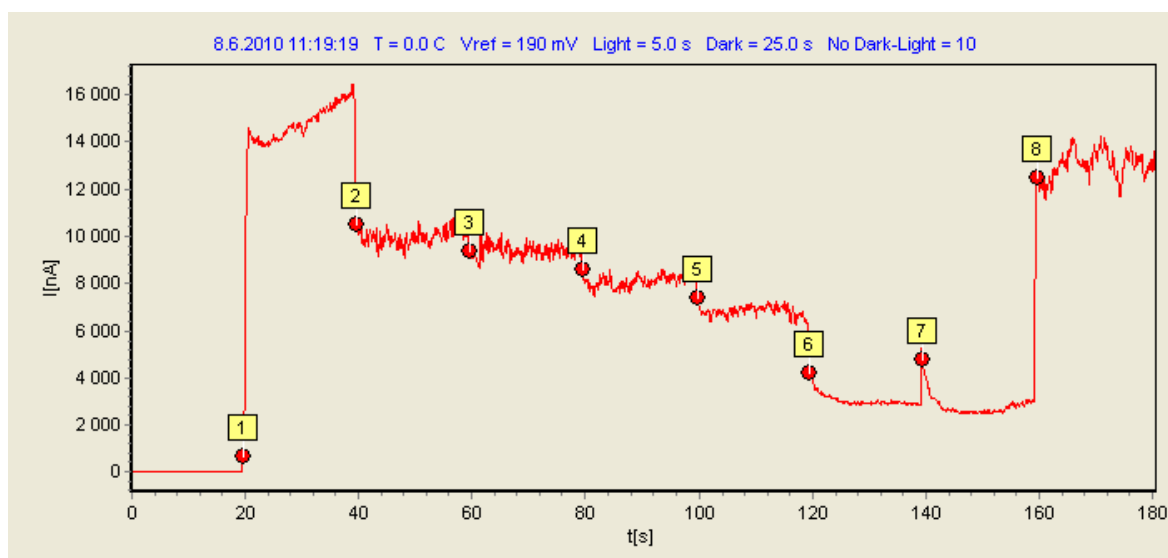

Fig. 15: Example of a record measured on the sensor 5 at a flow rate of 150 μl min^{-1} and the voltage of 2 V supplied to rotation component. Numbers in yellow squares show an electrode number on the array sensor. All measured graphs are provided on attached CD in the file "Optimization of rotation and flow speed.doc".

Fundamental problem was revealed: the system - flow cell FC9 and AC9 sensor - is unstable under non-optimum conditions. The most important variable that ensures stability / causes instability is gap width *h* between sensor and rotation component. Under non-optimum

conditions, the flow forced by centrifugal power, which is transmitted on liquid by viscous forces, is bigger than input analyte flow. Liquid is incompressible and continuity relation holds true, therefore return flow Q_x occurs at the electrode area (Fig. 16).
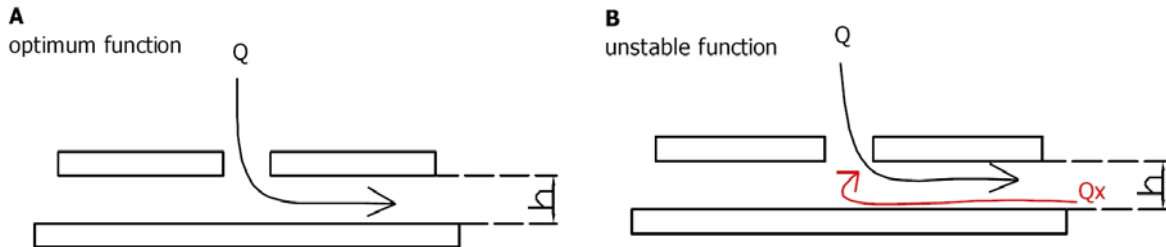

Fig. 16: Schematic diagram of a sensor with hole (through which the liquid flow Q enters) and a rotation component; A – system optimum function, B – unstable system function, where return flow Q_x occurs.

The return flow and its concentration are rather irreproducible. It develops from input analyte and output solution. It is clear if we realize that: *h* in current setup is 0.5-1 mm, the layer where the return flow occurs is about 0.1-0.3 mm and the diffusion reaction layer is 1-10 μm.

The instability does not have a turbulent character, because turbulence occurs at Re > 100 000 [40], [42]. It was found here that flow can suddenly change between optimum and unstable function at Re ≤ 1000, when both optimum and unstable flow are laminar. These phenomena are enabled in Navier-Stokes equations structure [44]. The solution of velocities field at zero flow is described by Weierstrass elliptic function [45], which is a periodic function. It implicitly proves the flow existence according to A and B schema (Fig. 16). Flow states with step changes were experimentally proved (Fig. 17). Current measured on eight electrodes of the array sensor AC9 should linearly grow with the square power of the voltage applied on motor controlling the rotation component speed. Instead, it suddenly jumps up at $U^2 = 3.24$ V^2 (Fig. 17). Such a non-linear behaviour was observed at different flow rates and on several sensors.
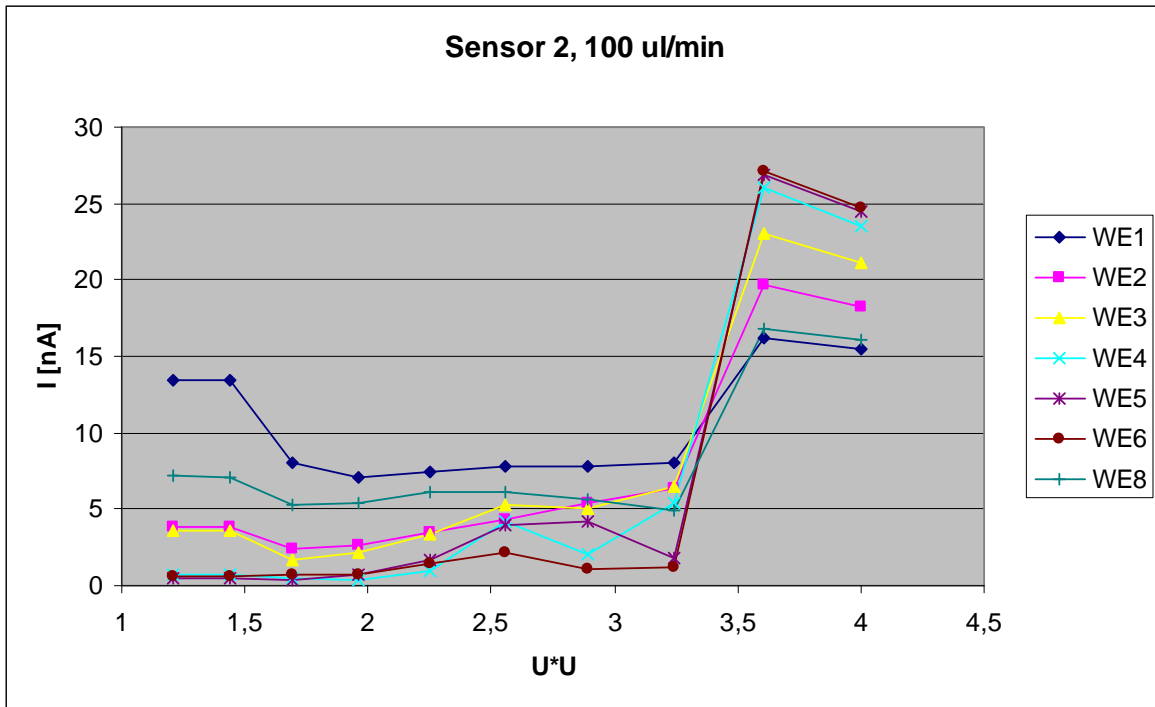
Fig. 17: Current response at particular working electrodes (WE1-WE8) of the AC9 electrochemical array sensor No. 2 on square power of voltage applied on motor of the rotating component at flow rate 100 µl/min.

5.2 Modelling the flow around sensor electrodes

Models of liquid flow in the FC9 cell around sensor electrodes show radial velocity distribution in the cell channels depending on rotation component – sensor electrodes distance h, flow rate in the input tubing Q and rotation component rotational speed. The values of Q and rotation component rotational speed were chosen to correspond to experimental values. Distance h was selected to fit current construction possibilities.

Tab. 3: Dependence of maximum radial velocity on the speed of rotation component, h and Q

Rotation component rotational speed	h = 0.1 mm Q = 100 µl/min	h= 0.1 mm Q = 200 µl/min	h= 0.2 mm Q = 100 µl/min	h = 0.2 mm Q = 200 µl/min
[rps]	Maximum radial velocity [m/s]			
0	7.5*10-3	0.02	4.1*10-3	8.2*10-3
100	11.9	11.9	5.8	5.9

51

It was found that the liquid flow rate Q change between 100 and 200 μl/min had negligible influence on the maximum radial liquid velocity (Tab. 3). On the contrary, the distance h, between the rotation component and sensor electrodes, remarkably changed the maximum radial velocity. The thinner was the distance between the rotation component and sensor electrode, the higher was the liquid radial velocity.
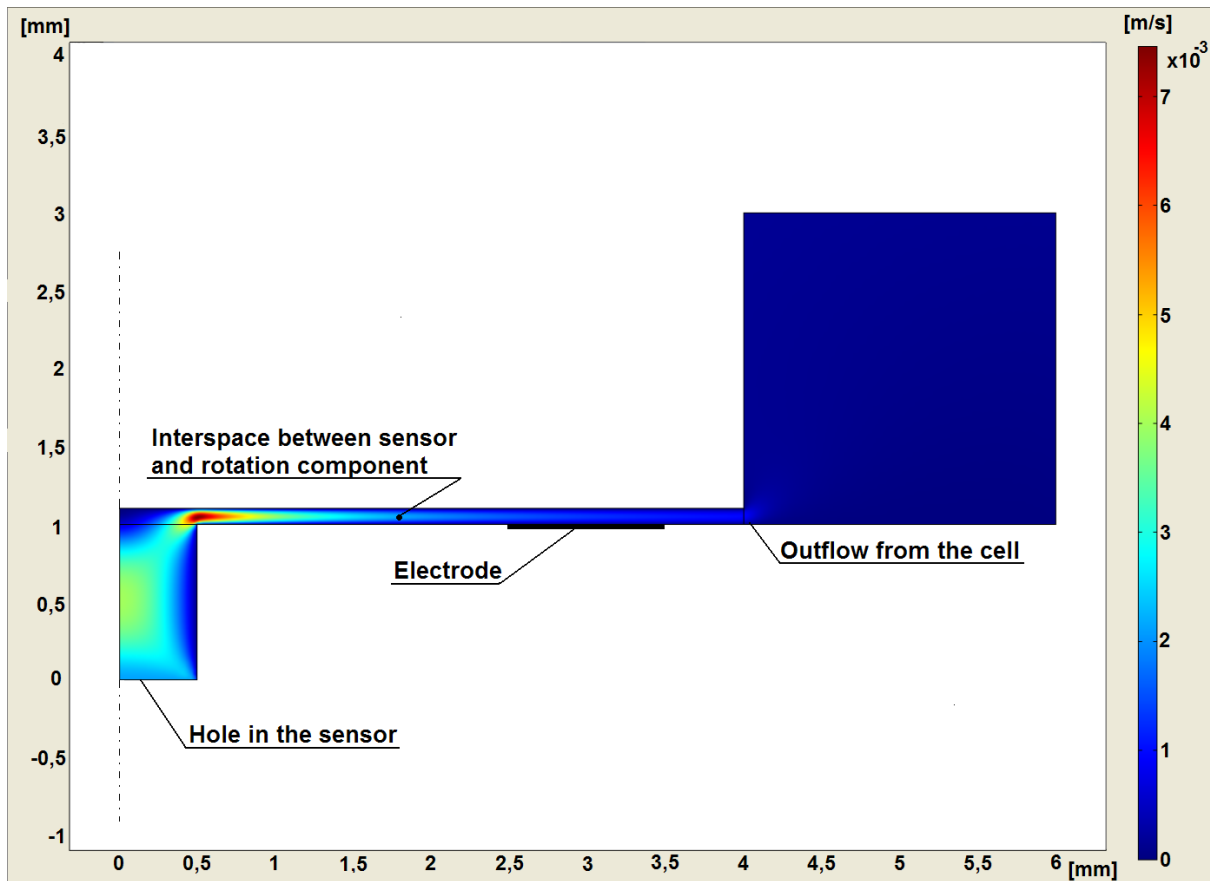

Fig. 18: Model of liquid flow in the FC9 cell with AC9 sensor. Rotation component rotational speed: 0 rps; i.e. the liquid is pumped by flow rate 100 μl/min. Rotation component – sensor electrodes distance h: 0.1 mm; maximum speed obtained $7.5*10^{-3}$ m/s.

Fig. 19: Rotation component rotational speed: 100 rps; rotation component – sensor electrodes distance: 0.1 mm; flow rate: 100 µl/min; maximum speed: 11.876 m/s

Fig. 20: Rotation component rotational speed: 0 rps; rotation component – sensor electrodes distance: 0.1 mm; flow rate: 200 µl/min; maximum speed: 0.0149 m/s

53
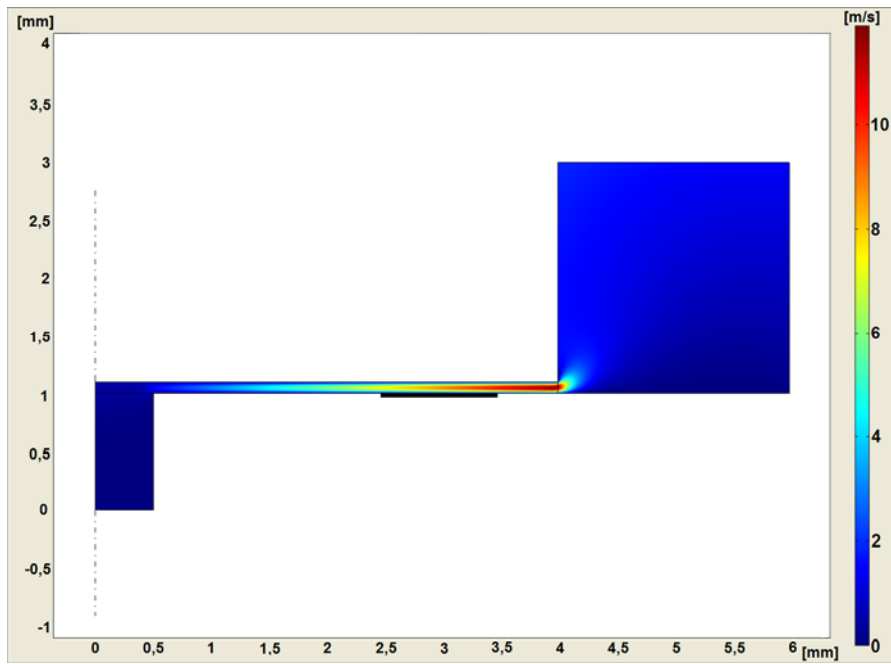
Fig. 21: Rotation component rotational speed: 100 rps; rotation component – sensor electrodes distance: 0.1 mm; flow rate: 200 μl/min; maximum speed: 11.881 m/s
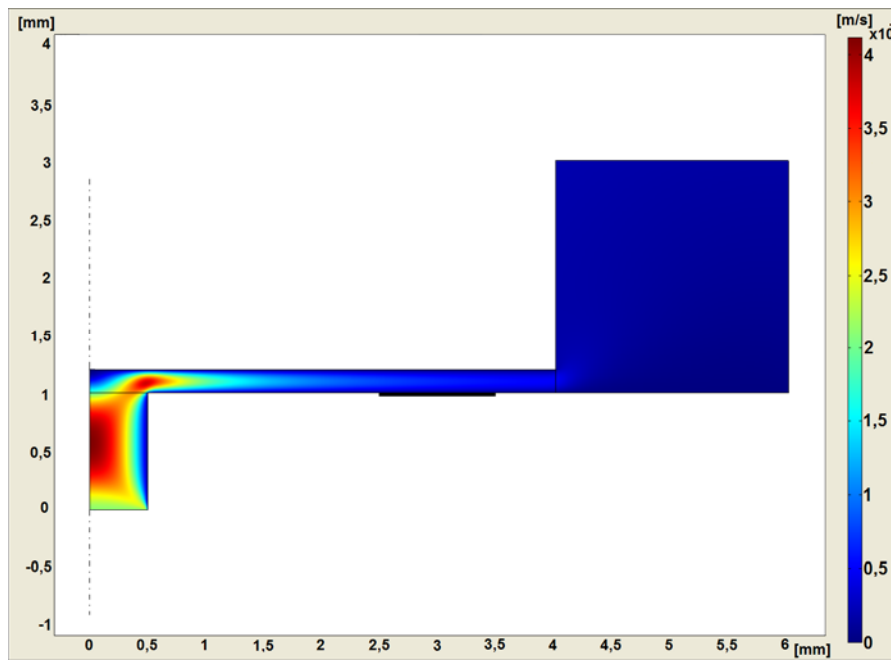
Fig. 22: Rotation component rotational speed: 0 rps; rotation component – sensor electrodes distance: 0.2 mm; flow rate: 100 μl/min; maximum speed: 4.112×10^{-3} m/s
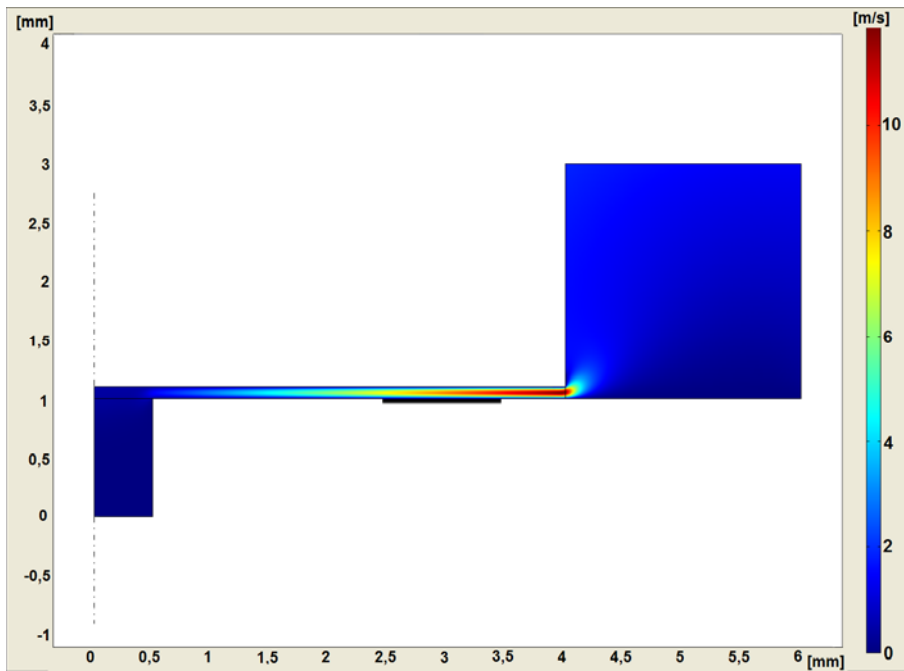
Fig. 23: Rotation component rotational speed: 100 rps; rotation component – sensor electrodes distance: 0.2 mm; flow rate: 100 μl/min; maximum speed: 5.839 m/s
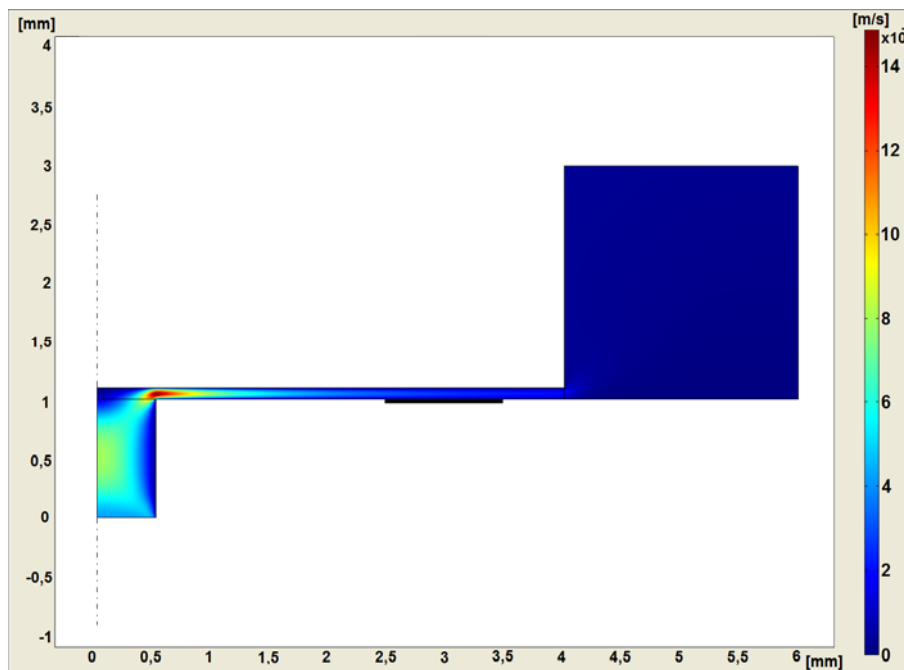

Fig. 24: Rotation component rotational speed: 0 rps; rotation component – sensor electrodes distance: 0.2 mm; flow rate: 200 μl/min; maximum speed: $8.224*10^{-3}$ m/s

55
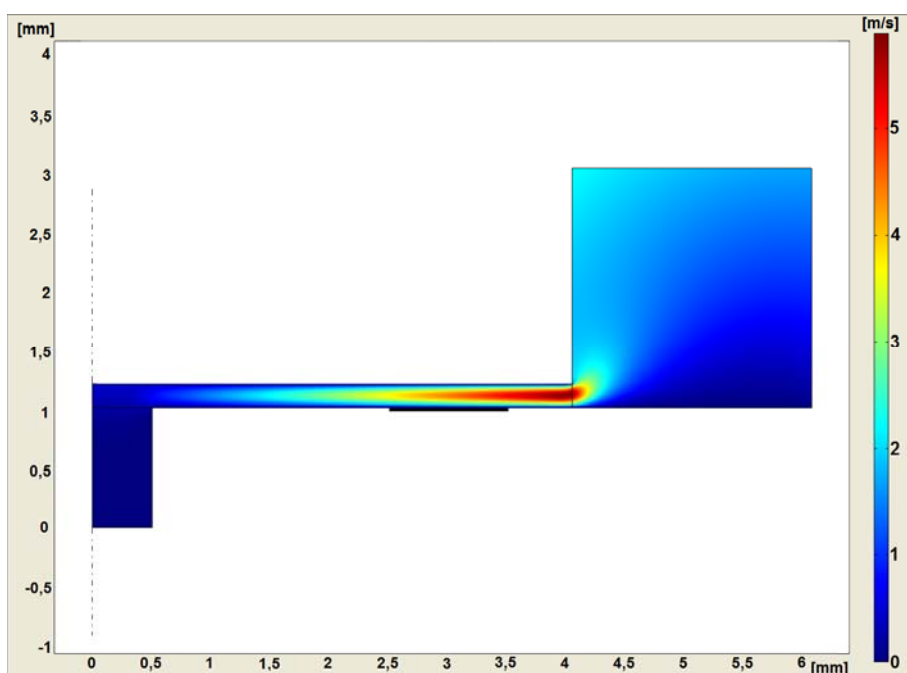
Fig. 25: Rotation component rotational speed: 100 rps; rotation component – sensor electrodes distance: 0.2 mm; flow rate: 200 μl/min; maximum speed: 5.887 m/s
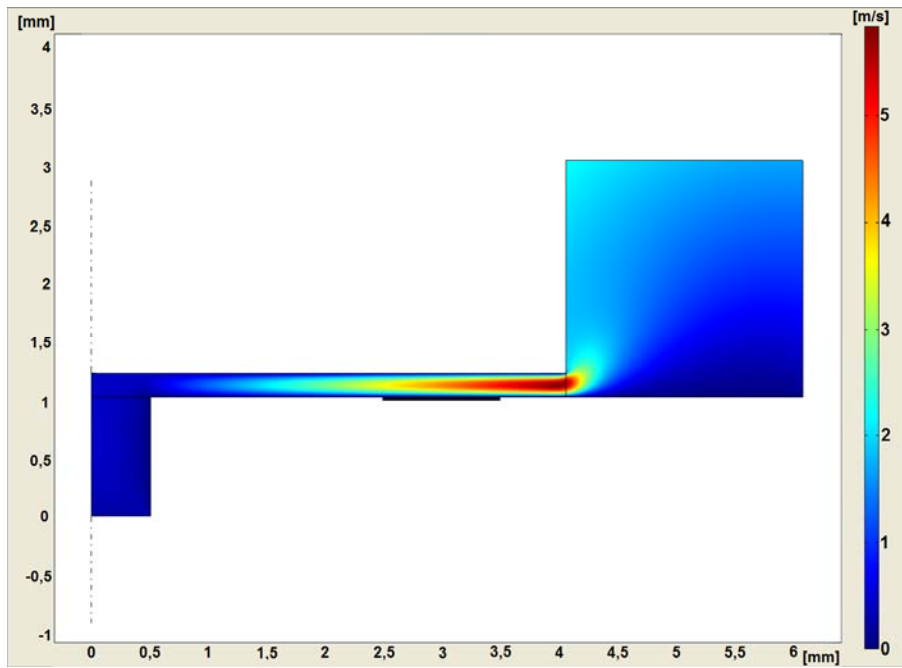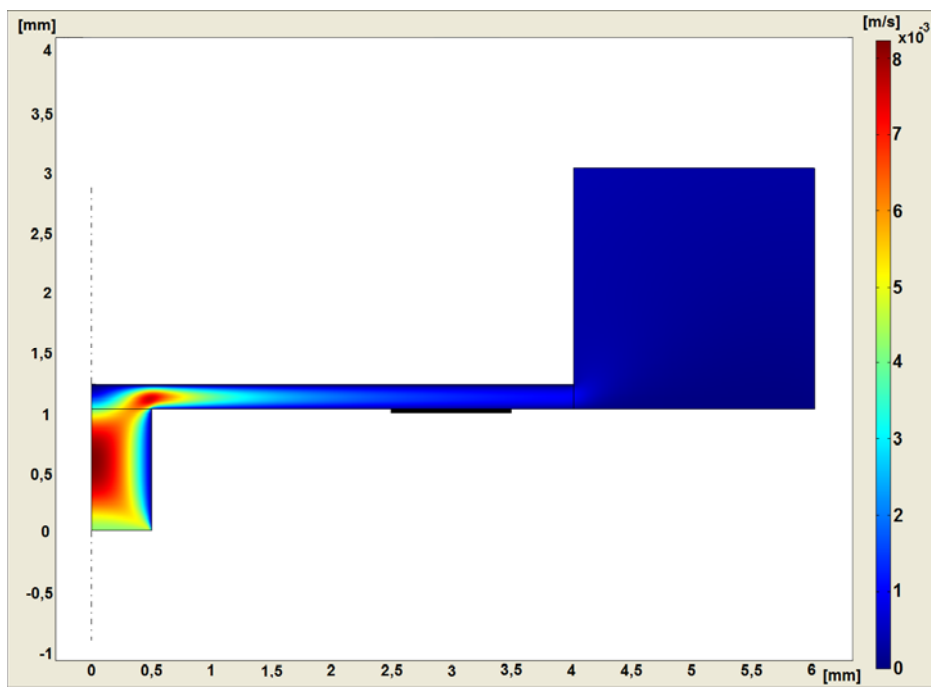
5.3 Array sensor with annular electrodes

Value of theoretical current under condition of 100% conversion was calculated as: $I = c*Q*F = 0.005$ [mol/l]$*1.67*10^{-6}$ [l/sec]$*96500$ [C/mol] $= 0.8$ mA. The highest measured current I_0 was 0.126 mA. It means that the electrode reaction conversion at the annular electrodes $(I_0/I).100$ was about **16%**. It is four times higher conversion value than measured on FC9 sensors. It is in agreement with working electrode geometric area of AC9 (0.78 mm^2) and annular electrode sensor (3.14 mm^2). Important result was that if I used six times lower flow rate, i.e. 5-10 μl/min, it would be possible to use annular sensor in coulometric mode of 100% analyte conversion.

I found that the annular electrodes 1, 2 and 3 (although possessing the same geometric area) provide different current values under the same conditions. The farther from the sensor hole, the higher signal (Fig. 26). It is logical, because angular velocity is growing from the middle towards the sensor edge. Thus, the result shows that the geometric areas of single electrodes can not be the same but it has to be adapted according to the position on the sensor.

56
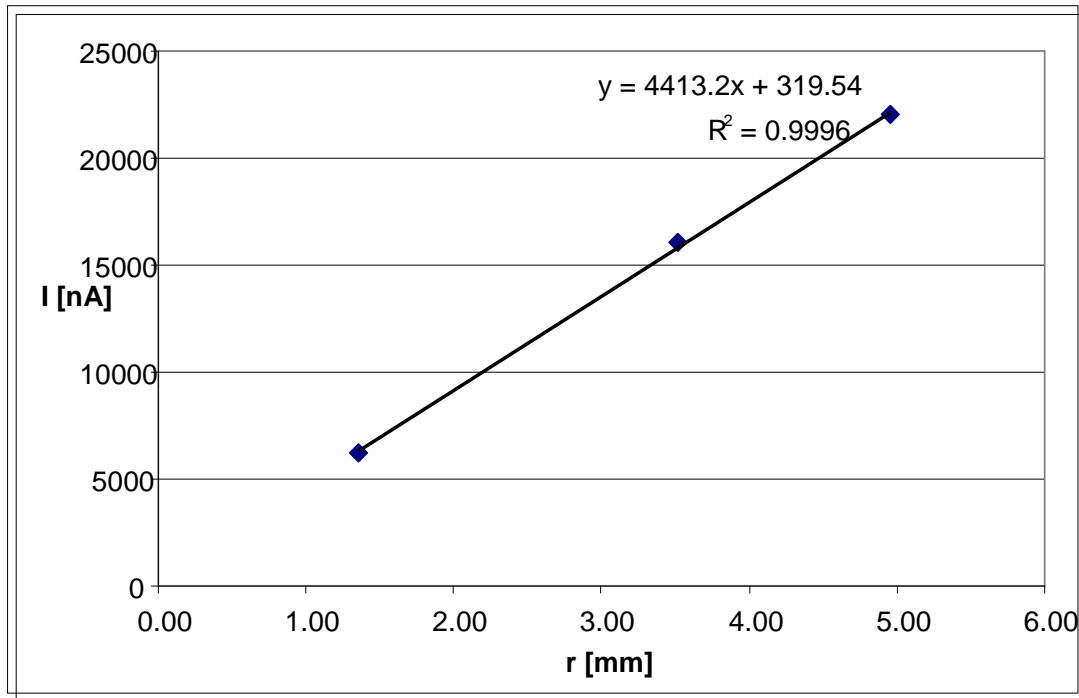
Fig. 26: Current dependence of 3 electrodes on their mean diameter: $r_1 = 1.35$ mm, $r_2 = 3.52$ mm, $r_3 = 4.95$ mm.

If the flow is stable, then the system with electrochemical sensor with annular electrodes will heavily increas mass transport between the electrodes and bulk solution. Within this work, 16% analyte conversion was reached at a flow rate of 100 µl/min. It is a rather positive result, which can be considered as a proof of the concept. If a very small flow rate of 5-20 µl/min is used, the annular electrode sensor can provide 100% conversion, i.e. coulometric function. One of the most important experimental results for the detector construction is, that electrode surface should be of minimum roughness and distance between rotation component and electrode surface should be minimum too. Equation (25) for radial velocity with the maximum F value 0,2 from the Fig. 8 gives relation for flow Q:

$$Q = 2\pi a^2 h 0.2\omega \tag{65}$$

Then *h* can be expressed as:

$$h = \frac{5Q}{2\pi a^2 \omega}. \tag{66}$$

57

Equation (66) serves for setting the right conditions to avoid flow instabilities.

The price of one annular sensor is about 100 CZK, the FC9 flow cell costs about 50 000 CZK and the potentiostat BA4 for signal reading and analysis including software is about 150 000 CZK. Therefore this equipment set-up is 4.5 times cheaper as compared with the basic price of similar instrument CoulArray®.

5.4 Case study

Here, I discuss results on performance of the electrochemical detector consisting of FC9 flow cell with AC9 array sensor in connection with a liquid chromatograph with reference to Chapter 4.5. The typical measured curve for ascorbic acid (AA) and dopamine (DA) mixture is provided in Fig. 27.
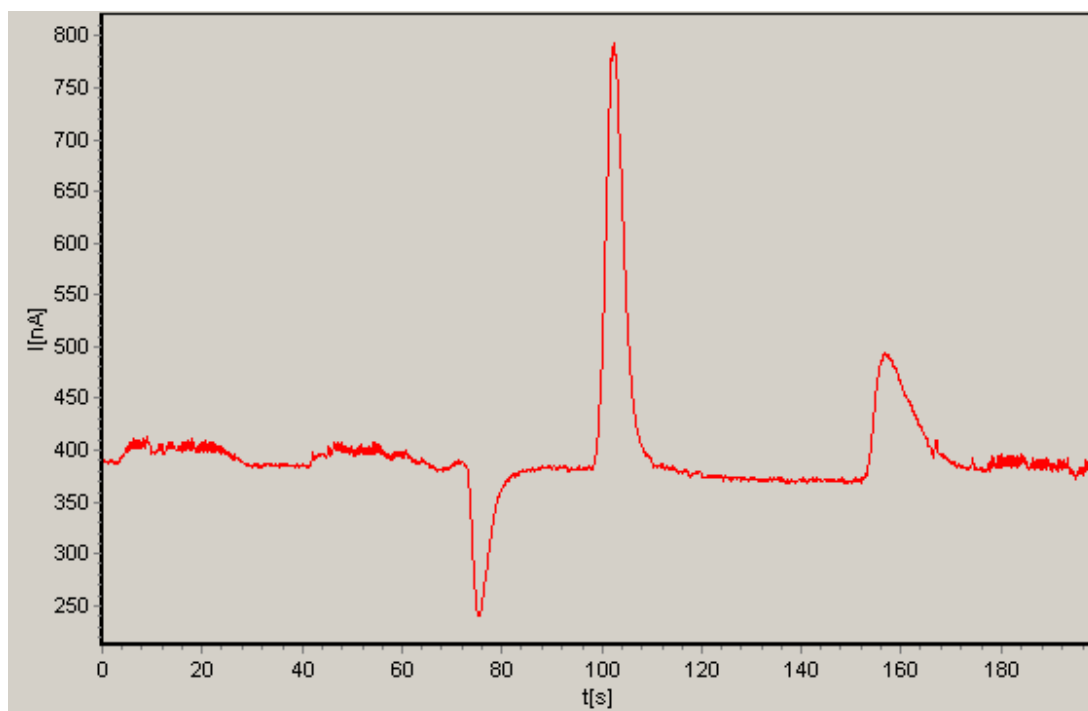
Fig. 27: Example of a chromatogram for 60 mM mixture of ascorbic acid (AA) and dopamine (DA) in 0.1% HCOOH (aq), pH 2.2. AA has retention time at 98 seconds, DA at 152 seconds. The negative peak at 73 s belongs to hydrochloric acid, which was included in the dopamine salt composition.

Firstly, DA and AA (each 1.1 mM) were measured separately on single electrodes of array sensor. The flow rate provided by a pump was 1 ml/min. Tab. 4 shows the AA and DA peak area measured on particular electrodes of the AC9 sensor. The standard deviation (SD) of the AA and DA peak was 18.3% and 24.5% respectively when measured on seven electrodes of the FC9 sensor. Electrode No. 7 was short-circuited.

Tab. 4: Comparison of peak area for 1.1 M AA and DA on single AC9 sensor

Electrode No	Peak area AA [nA^2]	Peak area DA [nA^2]
1	347372	292719
2	374294	288156
3	210980	154509
4	266634	191245
5	241259	166854
6	287589	231559
7	shortage	shortage
8	290101	180816
Average area	**288318**	**215123**
SD	52846	52612
SD [%]	**18.3**	**24.5**

The next step was measurement of AA and DA calibration curves. Their graphical and numerical evaluation is provided in the Fig. 28, Fig. 29, Fig. 30 and Tab. 5, Tab. 6 and Tab. 7. AA revealed linear range from $1*10^{-5} – 5*10^{-4}$ M. DA at low concentrations from $1.6*10^{-5}$ up to $2.5*10^{-4}$ M showed big dispersion, therefore its linear and dynamic range equals and it was not possible to evaluate limit of detection.
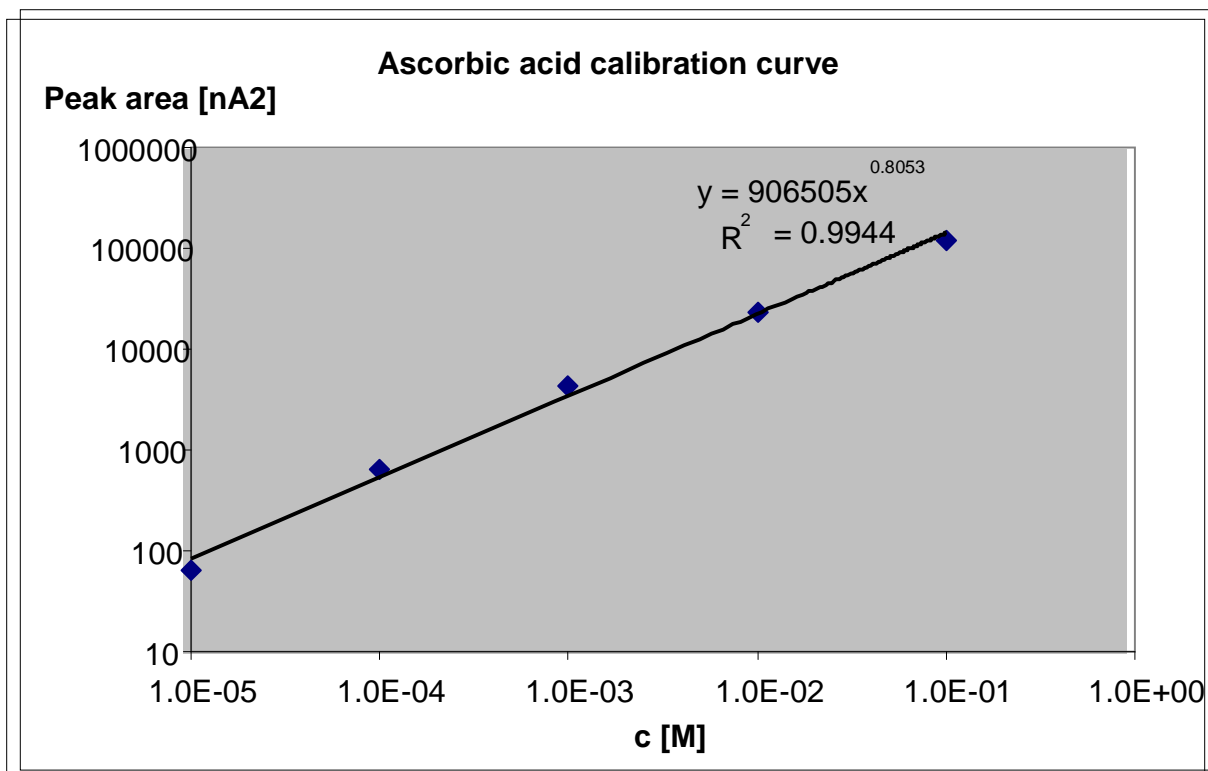
Fig. 28: AA calibration curve, non-linear part

Tab. 5: Concentration and peak area values from **Fig. 28**

c [M]	1.0E-05	1.0E-04	1.0E-03	1.0E-02	1.0E-01
Peak Area [nA^2]	**65.5**	**655.6**	**4373.6**	**23146.4**	**117231.4**
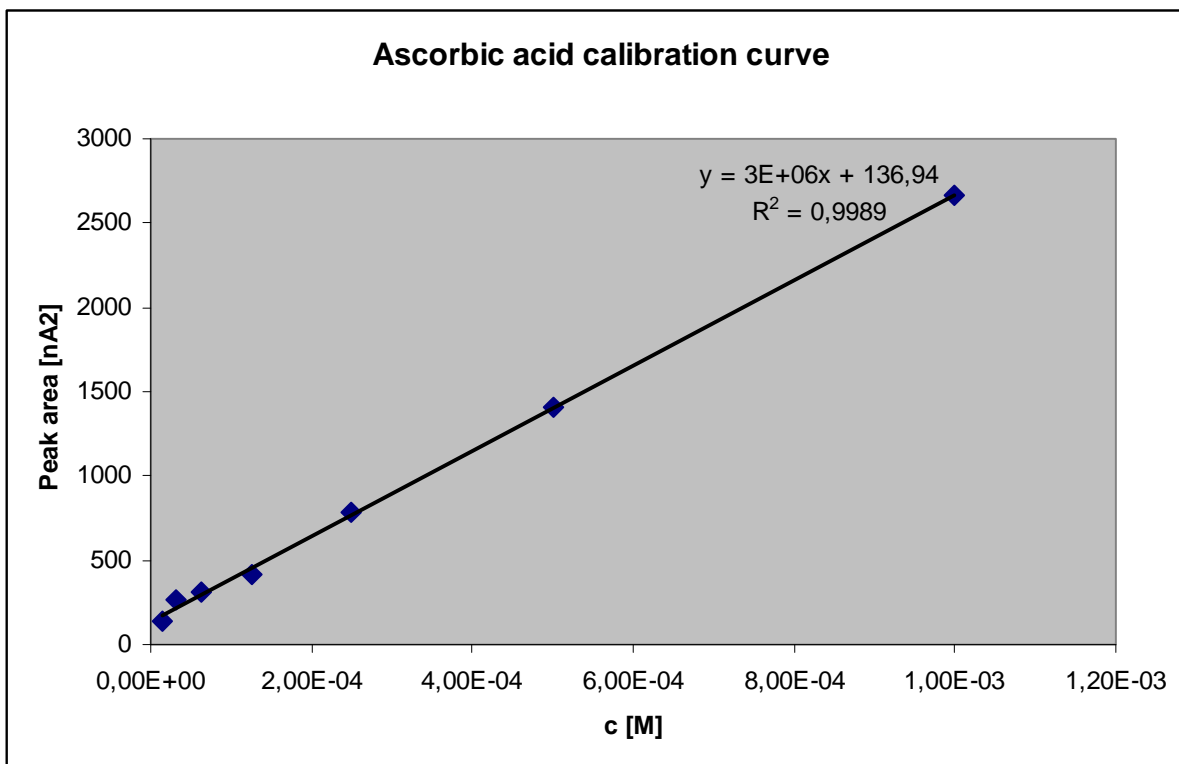
Fig. 29: AA calibration curve, linear part

Tab. 6: Concentration and peak area values from **Fig. 29**

c [M]	1.6E-05	3.1E-05	6.3E-05	1.3E-04	2.5E-04	5.0E-04	1.0E-03
Peak Area [nA^2]	**136.7**	**259.8**	**308.4**	**416.4**	**789.9**	**1404.9**	**2664.3**
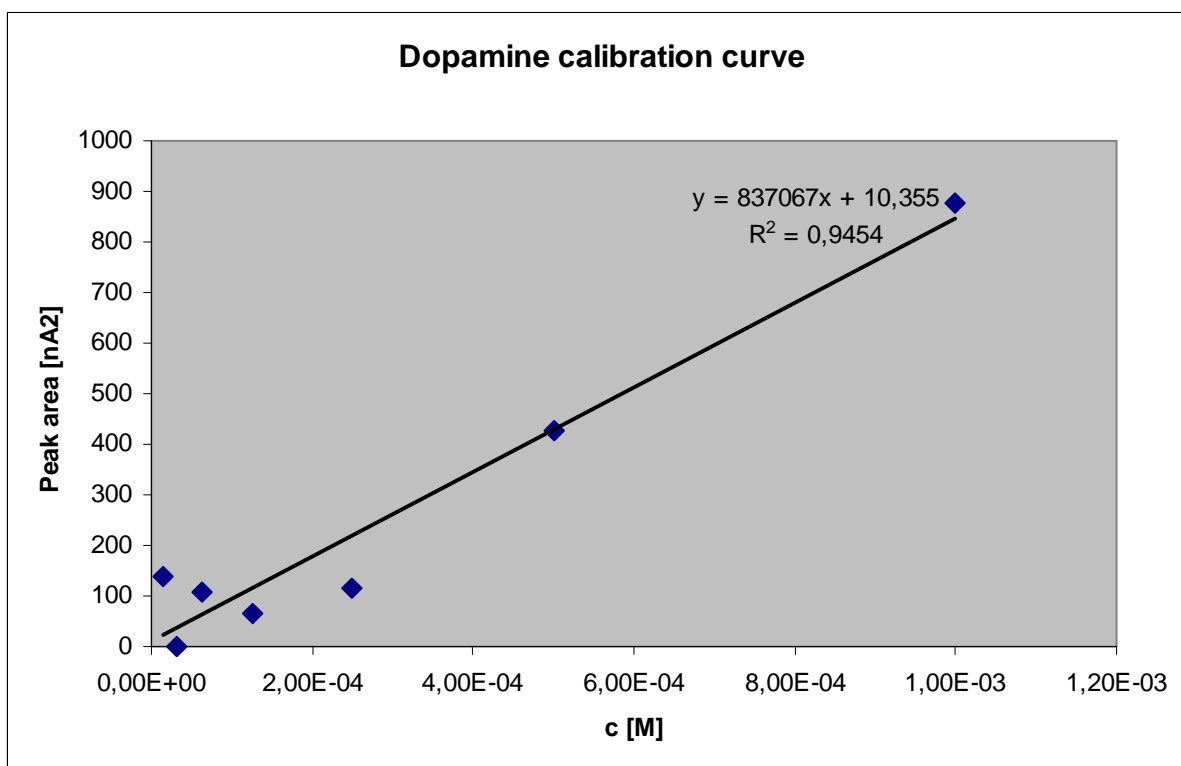
Fig. 30: DA calibration curve

Tab. 7: Concentration and peak area values from **Fig. 30**

c [M]	1.6E-05	3.1E-05	6.3E-05	1.3E-04	2.5E-04	5.0E-04	1.0E-03
Peak Area [nA2]	139.6	0	108.4	65.8	114.7	428.7	876.4

5.4.1 New detector specifications

Dynamic range: AA $1.56*10^{-5}$ – 0.1 M, DA $2.5*10^{-4}$ – 10^{-3} M

Linear range: AA 10^{-5} – $5*10^{-4}$ M, DA $2.5*10^{-4}$ – 10^{-3} M

Noise level: 0.3 nA

Minimum detectable concentration: AA $1.56*10^{-5}$ M, DA lack of points to evaluate

Time constant: 3 s

Operating temperature range: 5 – 40 ^{o}C

6 Conclusions

1. An electrochemical detector for liquid chromatography based on a screen-printed electrochemical sensor with an electrode array was designed, developed and tested. The hydrodynamics in the sensor/cell system was described and optimized.

2. Detector specifications, i.e. dynamic range, linearity, noise level, minimum detectable concentration, time constant, and operating temperature range, were measured and provided in the chapter 5.4.1.

3. The states with discrete transitions were identified in given detector setup, including experimental verification.

4. The principle of a flow cell with rotating element and electrochemical sensor arrays can perform reliably, if the condition (66) is fulfilled. Then it is possible to construct efficient electrochemical detectors based on the principle given above. If h is even smaller, then a value calculated from (66), the detector can work with high analyte conversion up to coulometric regime. On the other hand, the condition (66) is very demanding as regards detector production, which might impede and delay its practical implementation.

5. Novel annular array sensor was designed and tested. It showed four times higher analyte conversion compared to AC9 electrochemical array sensor. If this sensor was operated under 5-10 μl/min analyte flow rate, it would be possible to use it in coulometric mode of 100% analyte conversion.

List of symbols and abbreviations

a	radius of finite circular disk
AA	ascorbic acid
APCI-MS	atmospheric pressure chemical ionization–mass spectrometry
C	molar concentration, [mol/s]
c_0	concentration in the bulk of the solution
c_M	two-sided frictional torque coefficient
D	diffusion coefficient, [m^2/s]
d	ring electrode width [m]
D_0	diffusion coefficient at reference temperature
DA	dopamine
DHAA	dehydroascorbic acid
DNA	deoxyribonucleic acid
EC	electrochemical
ECD	electrochemical detector
ESI-MS	electrospray ionization-mass spectrometry
F	Faraday constant, 96 484,6 [C/mol]
HPLC	High performance liquid chromatography
$i(t)$	measured current (dependence on time) [A]
i_L	limiting current, [A]
IR	infra-red
J	diffusion flux [mol/m^2.s]
j	mass flux to the disk surface
k	Boltzmann constant, 1.38.10^{-23} J/K
h	rotation component – sensor electrodes distance [mm]
l	characteristic length
LC	liquid chromatography
LS	light scattering
m	frictional torque
M	two-sided frictional torque
MS	mass spectroscopy
n	number of moles, [mol]
NMR	nuclear magnetic resonance
PCB	polychlorinated biphenyls
PET	positron emission tomography
Q	flow rate [dm^3/s]
Q_x	return flow rate [dm^3/s]
R	internal radius of the tube [m]
r	cylindrical coordinate, diameter axis [m]
RDE	rotating disc electrode
Re	Reynolds number
RI	refractive index
ROS/RNS	reactive oxygen species/reactive nitrogen species
rpm	revolutions per minute

rps	revolutions per second
Sc	Schmidt number
Sh	Sherwood number
t	time
TLS	thermal lens spectroscopy
UA	uric acid
U_D	activation energy for diffusion [kJ/mol]
UV	ultra-violet
UV/Vis	ultraviolet/visible
U_υ	activation energy for viscosity [kJ/mol]
v	characteristic velocity
V_z	capture rate of the fluid by the disk
X_r	rotating disk electrode diameter [m]
y	vertical axis
δ	fluid layer thickness [m]
δ_0	thickness of hydrodynamic boundary layer on the disk surface
Δp	pressure difference between the two ends of the tube [Pa]
η	dynamic fluid viscosity [Pa.s]
v	fluid velocity, [m/s]
v_r	radial velocity component
v_y	axial velocity component
v_φ	tangential velocity component
π	mathematical constant
ρ	fluid density
τ	time constant
υ_0	viscosity at reference temperature
ω	angular frequency, [rad/s]

7　References

[1] http://www.chromatography-online.org/HPLC.html

[2] http://kerouac.pharm.uky.edu/ASRG/HPLC/Detectors.html

[3] V. R. Meyer, Practical High-Performance Liquid Chromatography, 4th Edition, Wiley-VCH Verlag GmbH & Co, KGaA, 2004

[4] E. Heftmann, Chromatography 6th edition, part A: fundamentals and techniques, Elsevier B.V., 2004

[5] E. Katz, R. Eksteen, P. Schoenmakers, N. Miller, Handbook of HPLC, Chromatographic science series, Vol. 78, Marcel Dekker, Inc., 1998

[6] R. J. Flanagan, D. Perrett, R. Whelpton, Electrochemical detection in HPLC: Analysis of drugs and poisons, The Royal Society of Chemistry, 2005

[7] E. Gileadi, Electrode Kinetics for Chemists, Chemical Engineers and Material Scientists, Wiley-VCH, Inc., 1993

[8] H. Parvez, M. Bastart-Malsot, S. Parvez, T. Nagatsu, G. Carpentier, Electrochemical detection in medicine and chemistry, (Progress in HPLC; vol. 2), VNU Science Press BV, 1987

[9] http://www.esainc.com/products/type/hplc_systems/detectors/coulochem

[10] A. Chmielewska, L. Konieczna, A. Plenis, H. Lamparczyk, Sensitive quantification of chosen drugs by reversed-phase chromatography with electrochemical detection at a glassy carbon electrode, *Journal of Chromatography B*, 839 (2006) 102–111

[11] T.A. Ivandini, B.V. Sarada, C. Terashima, T.N. Rao, D.A. Tryk, H. Ishiguro, Y. Kubota, A. Fujishima, Electrochemical detection of tricyclic antidepressant drugs by HPLC using

highly boron-doped diamond electrodes, *Journal of Electroanalytical Chemistry* 521 (2002) 117–126

[12] O. Kuhlmann, G. Stoldt, H.G. Struck, G.J. Krauss, Simultaneous determination of diclofenac and oxybuprocaine in human aqueous humor with HPLC and electrochemical detection, *Journal of Pharmaceutical and Biomedical Analysis* 17 (1998) 1351–1356

[13] C.S. Lai, N.K. Nair, A. Muniandya, S.M. Mansora, P.L. Olliarob, V. Navaratnama, Validation of high performance liquid chromatography–electrochemical detection methods with simultaneous extraction procedure for the determination of artesunate, dihydroartemisinin, amodiaquine and desethylamodiaquine in human plasma for application in clinical pharmacological studies of artesunate–amodiaquine drug combination, *Journal of Chromatography B*, 877 (2009) 558–562

[14] R. Nakao, K. Furutuka, M. Yamaguchi, K. Suzuki, Quality control of PET radiopharmaceuticals using HPLC with electrochemical detection, *Nuclear Medicine and Biology* 33 (2006) 441–447

[15] J. A. Rodriguez, E. Barrado, Y. Castrillejo, J. R. Santos, J. L.F.C. Lima, Validation of a tubular bismuth film amperometric detector. Determination of diclofenac sodium by multisyringe flow injection analysis, *Journal of Pharmaceutical and Biomedical Analysis* 45 (2007) 47–53

[16] A. Zerzanova, V. Zizkovsky, R. Kucera, J. Klimes, I. Jesensky, J. Dohnal , D. Barron, Using of HPLC coupled with coulometric detector for the determination of biotin in pharmaceuticals, *Journal of Pharmaceutical and Biomedical Analysis* 45 (2007) 730–735

[17] O. Chailapakul, W. Wonsawat, W. Siangproh, K. Grudpan, Y. Zhao, Z. Zhu, Analysis of sudan I, sudan II, sudan III, and sudan IV in food by HPLC with electrochemical detection: Comparison of glassy carbon electrode with carbon nanotube-ionic liquid gel modified electrode, *Food Chemistry* 109 (2008) 876–882

[18] J. Kac, T. Vovk, Sensitive electrochemical detection method for α-acids, β-acids and xanthohumol in hops (*Humulus lupulus* L.), *Journal of Chromatography B*, 850 (2007) 531–537

[19] D. Potesil, J. Petrlova, V. Adam, J. Vacek, B. Klejdus, J. Zehnalek, L. Trnkova, L. Havel, R. Kizek, Simultaneous femtomole determination of cysteine, reduced and oxidized glutathione, and phytochelatin in maize (*Zea mays* L.) kernels using high-performance liquid chromatography with electrochemical detection, *Journal of Chromatography A*, 1084 (2005) 134–144

[20] M. Skrinjar, M. H. Kolar, N. Jelsek, A. R. Hras, M. Bezjak, Z. Knez, Application of HPLC with electrochemical detection for the determination of low levels of antioxidants, *Journal of Food Composition and Analysis* 20 (2007) 539–545

[21] A. Ishida, M. Natsume, T. Kamidate, Microchip reversed-phase liquid chromatography with packed column and electrochemical flow cell using polystyrene/poly(dimethylsiloxane), *Journal of Chromatography A*, 1213 (2008) 209–217

[22] M. Takagi, Threading intercalation to double-stranded DNA and the application to DNA sensing. Electrochemical array technique, *Pure Appl. Chem.* 73 (2001) 1573–1577

[23] G. Cannazza, A. Di Stefano, B. Mosciatti, D. Braghiroli, M. Baraldi, F. Pinnen, P. Sozio, C. Benatti, C. Parenti, Detection of levodopa, dopamine and its metabolites in rat striatum dialysates following peripheral administration of l-DOPA prodrugs by mean of HPLC–EC, *Journal of Pharmaceutical and Biomedical Analysis* 36 (2005) 1079–1084

[24] J. Kehr, Determination of glutamate and aspartate in microdialysis samples by reversed-phase column liquid chromatography with fluorescence and electrochemical detection, *Journal of Chromatography B*, 708 (1998) 27–38

[25] R. Migheli, G. Puggioni, S. Dedola, G. Rocchitta, G. Calia, G. Bazzu, G. Esposito, J. P. Lowry, R. D. O'Neill, M.S. Desole, Egidio Miele, P. A. Serra, Novel integrated microdialysis–amperometric system for in vitro detection of dopamine secreted from

PC12 cells: Design, construction, and validation, *Analytical Biochemistry* 380 (2008) 323–330

[26] N. A. Santagati, G. Ferrara, A. Marrazzo, G. Ronsisvalle, Simultaneous determination of amphetamine and one of its metabolites by HPLC with electrochemical detection, *Journal of Pharmaceutical and Biomedical Analysis* 30 (2002) 247–255

[27] H. Carrero, J. F. Rusling, Analysis of haloacetic acid mixtures by HPLC using an electrochemical detector coated with a surfactant-nafion film, *Talanta* 48 (1999) 711–718

[28] M. Rancan, S. Rossi, A. G. Sabatini, Determination of Thiamethoxam residues in honeybees by HPLC with an electrochemical detector and post-column photochemical reactor, *Journal of Chromatography A*, 1123 (2006) 60–65

[29] N. A. Santagati, E. Bousquet, A. Spadaro, G. Ronsisvalle, Analysis of aliphatic amines in air samples by HPLC with electrochemical detection, *Journal of Phamaceutical and Biomedical Analysis*, 29 (2002) 1105-1111

[30] J. Nakamura, D. K. La, J. A. Swenberg, Nicked Apurinic/Apyrimidinic Sites Are Resistant to β-Elimination by β-Polymerase and Are Persistent in Human Cultured Cells after Oxidative Stress, *The Journal of Biological Chemistry*, 275, 25 (2000) 5323–5328

[31] H. Ohshima, I. Celan, L. Chazotte, B. Pignatelli, H. F. Mower, Analysis of 3-Nitrotyrosine in Biological Fluids and Protein Hydrolyzates by HPLC Using a Postseparation, On-line Reduction Column and Electrochemical Detection: Results with Various Nitrating Agents, *Biology and Chemistry* 3 (1999) 132–141

[32] Shigenaga, M. K.; Lee, H. H.; Blount, B. C.; Christen, S.; Shigeno, E. T.; Yip, H.; Ames, B. N. Inflammation and NO(X)-induced nitration: assay for 3-nitrotyrosine by HPLC with electrochemical detection. *Proceedings of the National Academy of Sciences* 94 (1997) 3211–3216

[33] S. Tan, R. Bose, M. Derrick, Hypoxia-ischemia in fetal rabbit brain increases reactive nitrogen species production: quantitative estimation of nitrotyrosine, *Free Radical Biology & Medicine* 30 (2001) 1045–1051

[34] X. Li, A. A. Franke, Fast HPLC–ECD analysis of ascorbic acid, dehydroascorbic acid and uric acid, *Journal of Chromatography B*, 877 (2009) 853–856

[35] L. Feltl, V. Pacakova, K. Stulik, K. Volka, Reliability of Carotenoid Analyses: A Review, *Current Analytical Chemistry*, 1 (2005) 93-102

[36] http://www.esainc.com/resources/Detector_tech/How_EC_works

[37] http://www.esainc.com/products/type/hplc_systems/detectors/coulochem

[38] http://www.esainc.com/products/type/hplc_systems/detectors/coularray

[39] http://en.wikipedia.org/wiki/Hagen–Poiseuille_equation

[40] V.G. Levich, Physicochemical Hydrodynamics, Prentice Hall, Inc., 1962

[41] T. v. Karman, Uber laminare and turbulente Reibung, *Zeitschrift fur angewandte Mathematik und Mechanik*, Vol. 1, No. 4 (1921) 233-252

[42] A.D. Polyanin, A.M. Kutepov, A.V. Vyazmin and D.A. Kazenin, Hydrodynamics, Mass and Heat Transfer in Chemical Engineering, London and New York, Taylor & Francis 2002

[43] E. Dock, A. Christenson, S. Sapelnikova, J. Krejci, J. Emnes, T. Ruzgas, A steady-state and flow-through cell for screen-printed eight-electrode arrays, *Analytica Chimica Acta* 531 (2005) 165–172

[44] M. Brdička, L. Samek, B. Sopko, Mechanika kontinua, Academia, 2005

[45] http://en.wikipedia.org/wiki/Weierstrass's_elliptic_functions

8 Appendix

Curriculum vitae

Name   Zuzana Sajdlová (born Grosmanová)

Date of birth 20 July 1979

Telephone   +420 608877572

E-mail   z.sajdlova@seznam.cz

Education

1990-1997   Grammar school of M. Koperník, Bílovec

1997-2002   Institute of Chemical Technology in Prague, Faculty of Chemical Technology, Specialization: chemical technology of metals and special inorganic materials, Diploma (Master's) degree

2005-today   University of South Bohemia in České Budějovice, Institute of Physical Biology, specialization: Biophysics, Ph.D. studies

Professional experience

2002-2004   Brno University of Technology, Dept. of Microelectronics, technician working on 2 national projects ANTOPE FD-K2/53 - development of biosensor toxicity analyser and IBIS FT-TA/089 – biosensors characteristics for detection of insecticides and photosynthesis inhibiting herbicides

2003-today   BVT Technologies, a.s., Brno – production of electrochemical sensors, biosensors and accessories. Manager of section "Trace Analysis using Biosensors" responsible for a product "Biosensor Toxicity Analyser"; customer service and advice on all BVT products; products and methods presentation at the conferences; participation in R&D projects.

8.1 List of presentations

Děd J., Novák P., **Grosmanová Z.**: Metody restaurování stříbrných sbírkových předmětů, Sborník z konzervátorského a restaurátorského semináře, 16.-18.9.2002 Brno, (poster and lecture, given by J. Ded)

Krejci J., Krejcova D., Sajdl O., **Grosmanova Z.**: Exact evaluation of electrochemical sensors (poster), 2nd International Workshop on Multianalyte Biosensing Devices, 18-20 February 2004, Tarragona, Spain (poster presented by Z. Grosmanova)

Krejci J., Krejcova D., Sajdl O., **Grosmanova Z.**: Electrochemical analysis of bioactive membranes properties, The Eight World Congress on Biosensors, 24-26 May 2004, Granada, Spain (poster presented by D. Krejcova)

Grosmanova Z., Krejci J.: Biosensoric Detection of Pesticides Ihibiting Acetylcholine Esterase, 48th CIPAC (Collaborative International Pesticides Analytical Council) Meeting and 3nd Joint FAO/WHO Meeting on Pesticides Specifications, 7 June 2004, Brno (lecture given by Z. Grosmanova)

Grosmanova Z., Krejci J., Tynek J.: Biosensoric detection of acetylcholinesterase inhibiting pesticides in food sample, Proceedings of The 11th Electronic Devices and Systems Conference, September 9 - 10, 2004, Brno, ISBN 80-214-2452-4 (poster presented by Z. Grosmanova)

Krejci J., **Grosmanova Z.**, Koutkova H.: Pycnometric electrochemical cell, Intern. Conference Instrumental Methods of Analysis, Modern Trends and Applications, October 2-6, 2005, Iraklion, Crete, Greece (poster presented by Z. Grosmanova)

Krejci J., Stejskalova R., **Grosmanova Z.**: Array of mercury microelectrodes, 4th Croatian Symposium on electrochemistry, 28.5. – 1.6.2006, Primošten, Croatia (lecture given by Z. Grosmanova)

8.2 List of publications

Grosmanova Z., Krejci J., Tynek J.: Comparison of two pesticide measurement methods: AChE inhibition using biosensor and chromatographic analysis, International Journal of Environmental Analytical Chemistry 2005, 85 (12-13), 885-893

ABSTRACT: Screen-printed biosensors with immobilized acetylcholine esterase (AChE) were used for measuring fruit and vegetable samples that had first been analysed using gas and high-performance liquid chromatography. The output signal for the biosensors is the current, which is used to calculate relative inhibition (RI), a measured quantity. RI is proportional to the inhibiting (toxic) effect of organophosphates and carbamates. Measurements with AChE biosensors are not easily reproducible. This problem is solved by the choice of an arbitrary toxicity standard of 1.25mM Syntostigmin. Measurements were evaluated by the ratio of the relative inhibition of the sample against the relative inhibition of Syntostigmin. Results obtained from the biosensor match those of chromatography in 19 out of 38 total measurements made and for nine out of 19 positive samples. The confirmation rate was 50%. Future work must check the limit of 0.1 and the independent control of inhibiting pesticides contents after measurements using the biosensor.

Krejci J., **Grosmanova Z.**, Krejcova D., Skladal P., Safar B.: Biosensor Detection of Organophosphorous Gases; Commercial and Pre-Commercial Cell Detection technologies for Defence against Bioterror, L.M. Lechuga et al. (Eds.), NATO Science for Piece and Security Series, Sub-Series E: Human and Societal Dynamics, Vol. 39, IOS Press 2008, ISBN 978-1-58603-858-8, ISSN 1874-6276 (book chapter)

ABSTRACT: The portable device BioNA for detection of organophosphorous and carbamate substances was developed and tested. The motivation to create such a device was people protection against terrorist attacks by chemical agents (sarin, soman, tabun, VX) and improvement of pesticides control in developing countries. The device consists of analytical block containing the biosensor and diffusion chamber where the toxic chemicals are transferred from sampled air to the circulating solution. The electrical and hydrodynamic circuits are connected together by insertion of the analytical block into the main body of the device. The main idea behind the device is concept of evaluation of nerve agents presence. It is not

measurement of concentration but evaluation of sample toxicity. BioNA device is not still completely finished but it is on such a technical level that it can be reliably decontaminated, it is compact and sufficiently robust to test the biosensor detection possibilities both in laboratory testing chambers and in field trials with real nerve agents spread around the device.

Krejci J., Lacina K., Vranova H., **Grosmanova Z.**, Microflow Vessel Improving Reproducibility and Sensitivity of Electrochemical Measurements, Electroanalysis 20, 2008, No.23, 2579–2586

ABSTRACT: A new microflow system was designed and developed for electrochemical measurements. The electrochemical electrodes prepared using thick film technology were used in this arrangement. Results of various measurements such as simple amperometric measurement on the example of H_2O_2 detection, measurement with glucose oxidase (GOx) biosensor, soluble enzyme activity measurement etc. carried out using this system are reported. It was observed that the sensitivity and reproducibility of the electrochemical measurements is improved significantly. The new device performance was proved on H_2O_2 detection, activity of GOx measurement and heavy metals detection (measured concentration range: H_2O_2 10^{-9} to 10^{-1} M, glucose 10^{-6} to 10^{-2} M, activity of GOx 10^{-1} to 10^{2} IU, heavy metals (Cu, Pb) 10^{-4} to 10^{-3} M). The microflow insert greatly reduces the overall size of the electrolyte vessel and measurements with sample quantity as low as 2 mL can be accomplished.

Krejci J.; **Sajdlova Z.**; Krejci J. Jr.; Marvanek T., Voltammetry under a Controlled Temperature Gradient. Sensors 2010, 10, 6821-6835

ABSTRACT: Electrochemical measurements are generally done under isothermal conditions. Here we report on the application of a controlled temperature gradient between the working electrode surface and the solution. Using electrochemical sensors prepared on ceramic materials with extremely high specific heat conductivity, the temperature gradient between the electrode and solution was applied here as a second driving force. This application of the Soret phenomenon increases the mass transfer in the Nernst layer and enables more accurate control of the electrode response enhancement by a combination of diffusion and thermal diffusion. We have thus studied the effect of Soret phenomenon by cyclic voltammetry measurements in ferro/ferricyanide. The time dependence of sensor response disappears when applying the Soret

phenomenon, and the complicated shape of the cyclic voltammogram is replaced by a simple exponential curve. We have derived the Cotrell-Soret equation describing the steady-state response with an applied temperature difference.

8.3 List of patent applications

Krejci Jan; **Grosmanova Zuzana**; Krejci Jan Jr.; Maderankova Denisa; Marvanek Tomas; Havlik Roman, Electrochemical sensor and biosensor and electrochemical measurement method, CZ patent application PV 2007-309 and international application PCT CZ2008/000048, Publ. No.: US 2010181211 (A1)

ABSTRACT: The invention relates to an electrochemical sensor or biosensor that contains a substrate which bears at least one working electrode and a heating element, optionally also a temperature measuring element. This electrochemical sensor or biosensor allows achievement of better mass transport towards the working electrode during the measurement process. The invention further relates to a method of electrochemical measurement using the sensor or biosensor of the invention.

Krejci Jan; **Sajdlova Zuzana**; Chroma Lenka; Vranova Hana, Electrochemical sensor comprising a substrate and an injection moulded reaction vessel and method of its manufacture, CZ patent application PV 2009-22 and international application PCT/CZ2009/000068, Publ. No.: WO 2010083783 (A1)

ABSTRACT: An electrochemical sensor is described, containing a sensor substrate and at least one set of electrodes comprising a working electrode, a reference electrode and optionally an auxiliary electrode, further containing at least one reaction vessel, which is tightly connected to the sensor substrate and inside which is located at least one working electrode, whereas at least a part of the sensor substrate forms a vessel bottom. The vessel can contain a lid and also other preferred embodiments are described. Further is described a method of manufacture of the electrochemical sensor with the integrated reaction vessel, particularly by injection moulding.